General Disclaimer

One or more of the Following Statements may affect this Document

- This document has been reproduced from the best copy furnished by the organizational source. It is being released in the interest of making available as much information as possible.

- This document may contain data, which exceeds the sheet parameters. It was furnished in this condition by the organizational source and is the best copy available.

- This document may contain tone-on-tone or color graphs, charts and/or pictures, which have been reproduced in black and white.

- This document is paginated as submitted by the original source.

- Portions of this document are not fully legible due to the historical nature of some of the material. However, it is the best reproduction available from the original submission.

JPL PUBLICATION 77-81

An Assessment of an F_2 or N_2O_4 Atmospheric Injection From an Aborted Space Shuttle Mission

National Aeronautics and
Space Administration

Jet Propulsion Laboratory
California Institute of Technology
Pasadena, California

JPL PUBLICATION 77-81

An Assessment of an F_2 or N_2O_4 Atmospheric Injection From an Aborted Space Shuttle Mission

R. T. Watson
P. E. Smokler
W. B. DeMore

April 15, 1978

National Aeronautics and
Space Administration

Jet Propulsion Laboratory
California Institute of Technology
Pasadena, California

Preface

The work described in this report was performed by the Earth and Space Sciences Division of the Jet Propulsion Laboratory, under the cognizance of the Space Storable Propulsion Systems Technology Program.

Acknowledgment

The authors wish to acknowledge very helpful assistance by Professor Yuk Yung of the California Institute of Technology in the calculation of atmospheric residence times, and in discussions related to other aspects of transport properties of the atmosphere.

Contents

Tables

Figures

Abstract

If a Space Shuttle flight must be aborted before attaining escape velocity, the propellant for the payload would be ejected into the stratosphere or the ionosphere (which includes the mesosphere and the thermosphere).

Assuming a linear relationship between the stratospheric loading of NO_x and the magnitude of the ozone perturbation, we have calculated the change in ozone expected to result from the space shuttle ejection of N_2O_4, based on the ozone change that is predicted for the (much greater) NO_x input that would accompany large-scale operations of SSTs. These calculations show that the effect on ozone is negligibly small.

The N_2O_4 may also be released in the ionosphere. Because of the localized and transient nature of the effects, it is concluded that this will result in no adverse environmental impacts.

We have critically reviewed possible stratospheric fluorine reactions to evaluate the magnitude of fluorine-induced ozone destruction relative to the reduction that would be caused by addition of an equal amount of chlorine. The predicted effect on stratospheric ozone is vanishingly small.

A similar evaluation was made for an ionosphere injection. No adverse environmental impacts are predicted.

An Assessment of an F_2 or N_2O_4 Atmospheric Injection From an Aborted Space Shuttle Mission

I. Introduction

A. Objectives of the Report

The purpose of this report is to evaluate the potential for environmental impacts of possible Space Shuttle (SS) payload propellants that might be dumped in the stratosphere or ionosphere during a return-to-launch-site (RTLS) aborted mission.

Reflecting the awareness and concern of scientists and engineers for the environment, major technological undertakings are now preceded by assessments of effects on the environment to allow for planning, research, and design changes to mitigate such impacts. Recently, one area of particular concern has been the ozone-containing stratospheric layer protecting our planet's surface from harsh and biologically di[illegible] types of solar radiation (Ref. 1). Some scientists believe the ozone layer is threatened by high-flying commercial airliners (supersonic transports – SSTs) and chlorofluoromethanes (fluorocarbons), and therefore atmospheric modeling and chemistry have become the subjects of an intensive worldwide research effort to quantify such effects (Ref. 2).

While the potential for damage from these sources is still being evaluated, the fragile nature of the upper atmosphere has become common knowledge (Ref. 3). As such, it was realized that large-scale aerospace projects injecting exhaust gases into the Earth's upper atmosphere presented a potential hazard to the natural atmospheric balance (Ref. 4). The intent of this investigation has been to estimate the magnitude of this potential for one aspect of the SS project.

Since its developmental stages, various aspects of the SS project have been subject to impact assessment. Included among these are NO_x generation from SS reentry heat (Ref. 5), HCl exhaust gases from SS booster motors (Ref. 6), and others (Refs. 4, 7, and 8).

This report assesses another dimension of the SS project: the potential impacts from unburned propellant jettisoned in the stratosphere or ionosphere when an SS mission is aborted before escape velocity is attained.

The major portion of this report deals with the chemistry and modeling of N_2O_4 and F_2 injections into the stratosphere and ionosphere. Both chemical species are treated independently because they represent not a mixture of SS fuel, but the principal constituents of two fuels being considered for various payload packages of the SS. While other SS assessments have considered the case of 60 flights (and injections) annually, injections in this report are modeled as single, independent events because the concern of this report is restricted to aborted missions. While it is felt that a series of injections of this type could be simulated by a simple "scaling-up," such a

treatment is superfluous because any such series of mission failures would soon result in design changes.

B. Atmospheric Characteristics

The Earth's atmosphere, while consisting of gases, is nonuniform in terms of temperature, pressure, and composition. Ambient temperature has a range of over 400 K. At the surface of the Earth, temperatures average about 290 K and then decrease with altitude due to adiabatic cooling. However, at about 17 km, the altitude-temperature relationship reverses and the temperature begins to increase with altitude as a result of the presence of the ozone layer. In fact, there are three such temperature inflections in the atmosphere that occur at about 17, 50, and 85 km. The region below 17 km is the troposphere. This region is neglected in the remainder of this discussion because no injections would take place in that atmospheric layer. However, the troposphere is important and different from other regions of the atmosphere in that it is wet (high H_2O content). This gives rise to a major atmospheric removal process for many impurities by heterogeneous rainout. These temperature inflections, or inversions, result in stratification of the atmosphere into layers as illustrated in Fig. 1. This stratification is important in that it results in very slow vertical mixing of atmospheric constituents, so that the different layers of the atmosphere exhibit different characteristics. The extent of the variation in atmospheric constituents with respect to altitude can be seen in Fig. 2.

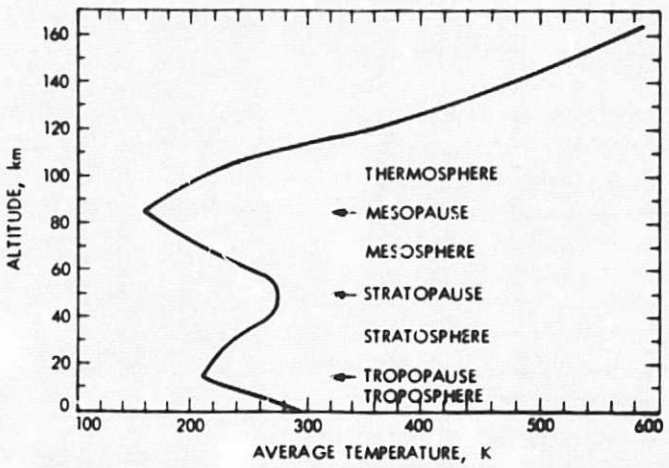

Fig. 1. Thermal profile of the atmosphere

Not only do the layers differ in temperature and specific atmospheric constituents, they also differ in the type of chemistry that predominates. The important chemistry in the stratosphere is homogenous, neutral chemistry dominated by radical species of the HO_x, NO_x, and O_x families. Perhaps the most significant constituent of the stratosphere is ozone, O_3, which shields the Earth's surface from ultraviolet (UV) light. The maximum concentration of atmospheric ozone is observed in the stratosphere at about 25 km.

Above the stratosphere are the mesosphere and thermosphere, as seen in Fig. 1. This region above 60 km, also collectively called the ionosphere, is usually further subdivided into three regions. The D region is from 60 to 90 km, and ionization there results primarily from the photoionization of NO ($NO + h\nu \rightarrow NO^+ + e$). Between 90 and 120 km is the E region, where photoionization of O_2 is the most important ion-forming step ($O_2 + h\nu \rightarrow O^+ + e$). In the F region, above 120 km, O, O_2, and N_2 all photoionize, ($O + h\nu \rightarrow O^+ + e$, and $N_2 + h\nu \rightarrow N_2^+ + e$) (Ref. 9).

The approaches used in this assessment reflect the major concerns for the different atmospheric layers, which are, in turn, a function of the dominant characteristics of the atmospheric region. The important characteristic of the stratosphere, for the present purpose, is the ozone content; therefore, the principal direction of the analysis for the stratospheric injection is the impact on the ozone concentration. Analogously, the assessment of the ionospheric region is principally concerned with the effects of a propellant release on the concentrations of the dominant ions. Certain unique features of high-altitude neutral chemistry were also considered.

II. Injection of the Propellant

A. Injection Parameters

The opportunities for fuel dumping within the flight plan for an RTLS abort mode are limited by competing operations of higher priority, as well as factors affecting the safety of the crew and vehicle. Such considerations restrict times of dumping to 153 to 363 s, 442 to 654 s and 744 to 984 s after liftoff, as summarized in Table 1. These three time spans are designated Segments I, II, and III. In the final RTLS flight plan, all three flight segments may be retained as alternates, or one specific initiation time may be chosen. In this report, propellant dumping is evaluated for all three flight segments as well as for dump durations of 50 s, 100 s, and 200 s.

Representative initial plumes that would result from these candidate initiation-duration combinations are schematically depicted in Fig. 3, a graph of the SS altitude as a function of ground-elapsed time (GET). The principal effects of the dumping duration are those of plume volume and initial dilution of the propellant, as well as definition of the layers of the atmosphere that the plume traverses. Velocity of the vehicle has a similar effect on initial concentrations. Trajectory guidelines are summarized in Table 2. Additional detail is available elsewhere (Ref. 10).

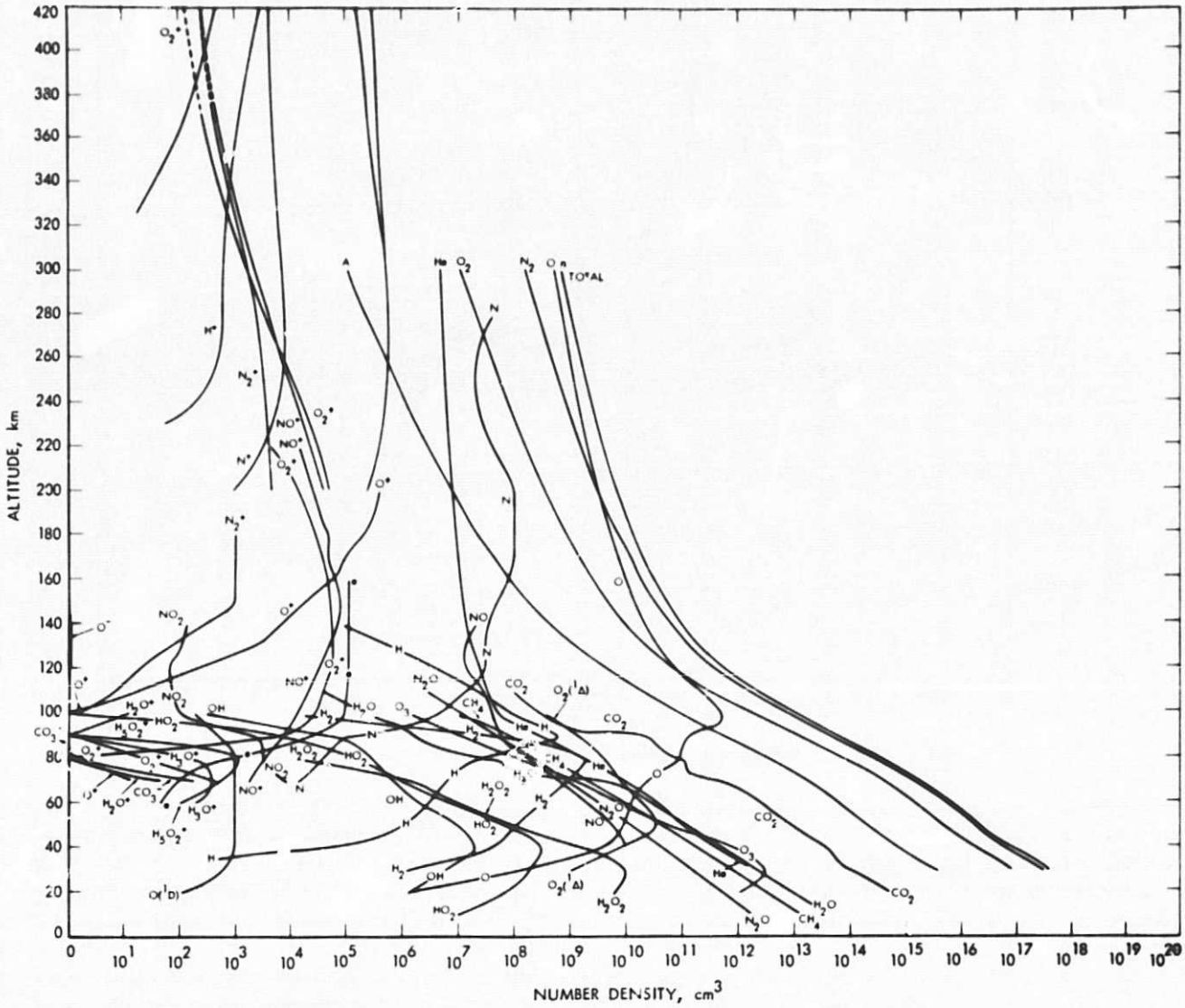

Fig. 2. Concentrations of chemical species in the atmosphere according to altitude

Table 1. RTLS flight plan segments satisfying criteria for propellant dumping

Flight Segment	RTLS events	GET, s	Altitude, km (ft)
I	Time of abort to pitch around	152.9 to 362.9	62.2 to 125.3 (203,976 to 411,188)
II	Maximum range distance to MECO	442 to 654	91.4 to 70.0 (300,000 to 229,756)
III	g acceleration control to Mach No. 3	744 to 984	42.9 to 28.5 (140,890 to 93,458)

The two particular SS payload propellants being evaluated contain 2722 kg (6,000 lb) of F_2, or 3402 kg (7,500 lb) of N_2O_4. For either propellant, this is a worst case analysis with regard to quantity in that lesser, but not greater, amounts of these substances may eventually be carried by the SS payload.

In terms of relevant aspects of the injection altitudes, all of the initiation-duration dumping options may be generalized as two cases. Dumps in Segments I and II would be restricted entirely to the ionospheric layer of the atmosphere, which includes portions of the mesosphere and the thermosphere. Any injections in Segment III would be restricted to the stratospheric layer. Hence, the two injection cases evaluated were an ionospheric injection and a stratospheric injection.

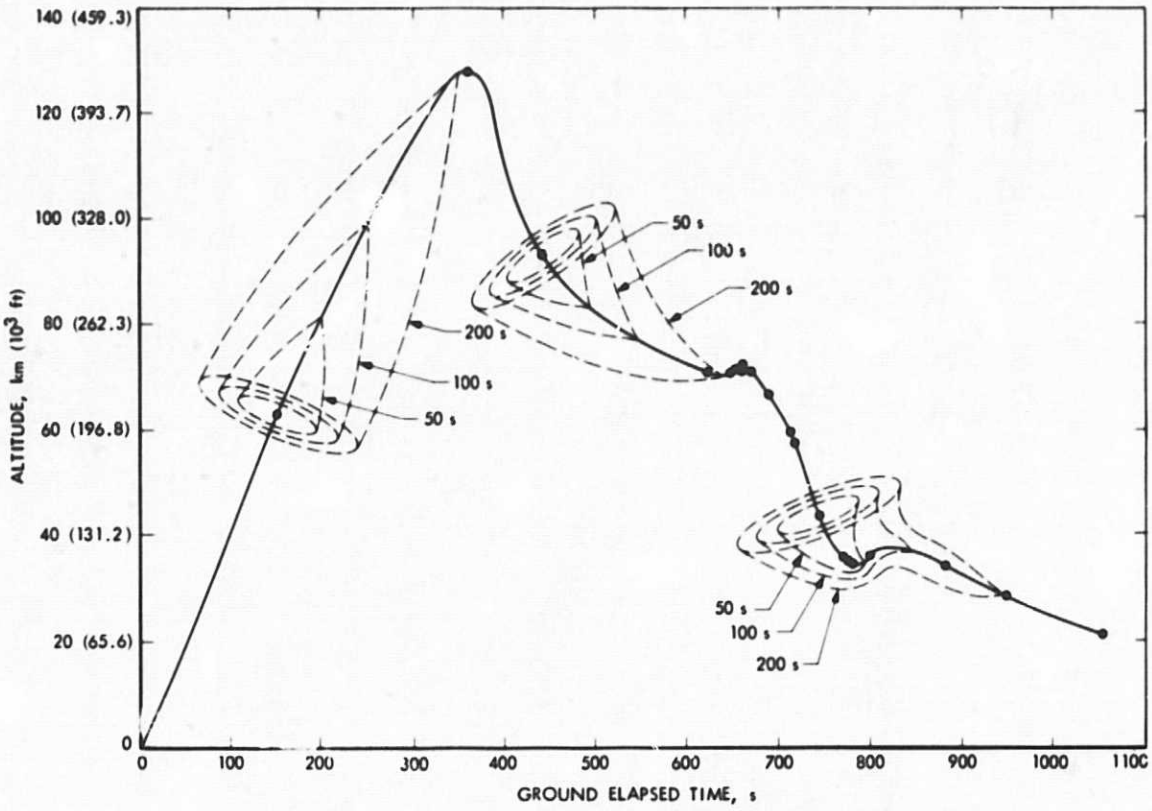

Fig. 3. Trajectory of the Space Shuttle during an RTLS abort

Those chemical species conceivably decreased by the injected propellant include stratospheric ozone and ionospheric charged particles. The magnitude of any perturbation to the ambient atmosphere would be dependent upon the concentration of the pollutant, which is a function of the absolute amount of the injected material and the rate of dilution due to transport processes. After a period of weeks to months, steady state (equilibrium) conditions would be reached and the injectant will have hemispherically dispersed. During this same time period, very little vertical transport will have occurred. Therefore, the steady-state concentration of the propellant merely reflects the height of the altitude regime into which the injection took place.

On a shorter time scale, before the plume hemispherically disperses, pollutant concentrations will be substantially higher, as will be the accompanying transient and localized perturbations. An evaluation of atmospheric diffusion parameters has been made in an attempt to estimate the time scale of the plume dispersal and the intermediate propellant concentrations.

B. Plume Dynamics

The main effects of fluid motions on atmospheric injectants are zonal (E-W) and meridional (N-S) circulatory advection, and turbulent eddy diffusion. The primary effect of the circulatory advection is simple horizontal displacement, whereas turbulent eddy diffusion causes dispersion of the injectant. In the stratosphere and mesosphere, the horizontal velocities (~1 to 100 ms^{-1}) are one to six orders of magnitude greater than the vertical velocities (~10^{-4} to 10^{-1} ms^{-1}), and are not constant at different altitudes with respect to velocity or direction (Ref. 11). The wind parameters abruptly change as is seen in Fig. 4 (Ref. 12). The effect of these abrupt changes is one of vertical stratification. Dispersion of the injectant is produced by both small and large scale eddies (in the stratosphere and mesosphere), and can be parameterized in terms of an overall eddy transport coefficient (K) by assuming that the eddy flux (F_a) is proportional to the gradient of the mean concentration of the pollutant being diffused (∇n_a), such that

$$F_a = -K\nabla n_a$$

Theoretical values of the horizontal (K_{yy}) and vertical (K_{zz}) eddy diffusion coefficients are available in the literature, based on the observed distributions of trace gases such as O_3, H_2O, N_2O, CH_4, and radioactive debris. Figure 5 shows typical values of K_{yy} and K_{zz} generated in a two-dimensional model (Ref. 11). It can be seen from these values of K_{yy} (~3×10^9

Table 2. RTLS abort; event sequence data

Event	GET, s	Relative velocity V, km/s (ft/s)	Altitude h, km (ft)
Time of abort	152.9	1.38 (4515)	62.17 (203,967)
Turn around	362.9	2.55 (8350)	125.33 (411,188)
3-g's acceleration	622.9	1.43 (4706)	69.67 (228,588)
Pitch down	649.9	2.07 (6781)	69.40 (227,676)
Main engine cutoff (MECO)	654.4	2.19 (7193)	69.81 (229,022)
External tank separation (ET SEP)	661.4	2.26 (7405)	70.03 (229.756)
ET SEP	661	2.26 (7405)	70.10 (229,998)
Pitch up	671	2.26 (7410)	69.61 (228,383)
Angle of attack, α_R	691	2.27 (7449)	65.85 (216,047)
Dynamic pressure, q = 20	712	2.27 (7463)	58.43 (191,669)
Mach No. = 7	716	2.27 (7459)	56.66 (185,891)
g acceleration control	744	2.16 (7092)	42.94 (140,890)
Mach No. = 6	771	1.85 (6058)	34.95 (114,680)
Maximum $\bar{q}$	774	1.81 (5946)	34.65 (113,689)
Pull out (γ = 0)	781	1.73 (5681)	34.37 (112,771)
Mach No. = 5	799	1.55 (5081)	35.79 (117,411)
Mach No. = 4	883	1.22 (4032)	34.03 (111,634)
Mach No. = 3	948	0.90 (2950)	28.48 (93,453)
Terminal augmented energy management (TAEM)	1054	0.46 (1499)	21.24 (69,689)
Autolanding	1375	0.17 (544)	2.67 (8,754)
Landing	1441	0.09 (295)	

$cm^2 \cdot s^{-1}$) and K_{zz} (~1 to 20 × 10^3 $cm^2 \cdot s^{-1}$) that horizontal mixing is significantly more rapid than vertical mixing. However, the actual diffusion coefficient values used in atmospheric models vary considerably, as is evident from Fig. 6, a graph of K_z coefficients used by different groups in their one-dimensional models. Figure 6 also illustrates the variation in K_z with altitude.

The vertical diffusion coefficient, K_z, can be used to calculate the residence time, which is an indication of how long the pollutant will remain in the atmosphere. The residence time is defined as the time it takes for the amount of the pollutant that remains in the atmosphere to decrease to 1/e of the original amount (the e-folding time). These calculations normally assume that the lifetime in the troposphere is short (a few days) and controlled by heterogeneous rain-out processes. Figure 7 is a graph of the residence times calculated from the profiles shown for K_z in Fig. 6. It can be seen that the predicted residence times in the Chang and McElroy, et al., models (Ref. 13) differ by about 8 years for an injection at 45 km. This illustrates the importance of the K_z profile chosen. If the McElroy, et al., profile is used, there is essentially no difference in residence time between a 22-km injection and a 45-km injection. However, K_z values used in the Chang model result in a difference in residence time of over 10 years for those same injections. Relative to the McElroy, et al., model, the Chang model would predict a longer residence time for mesospheric injections. Recently, however, the consensus

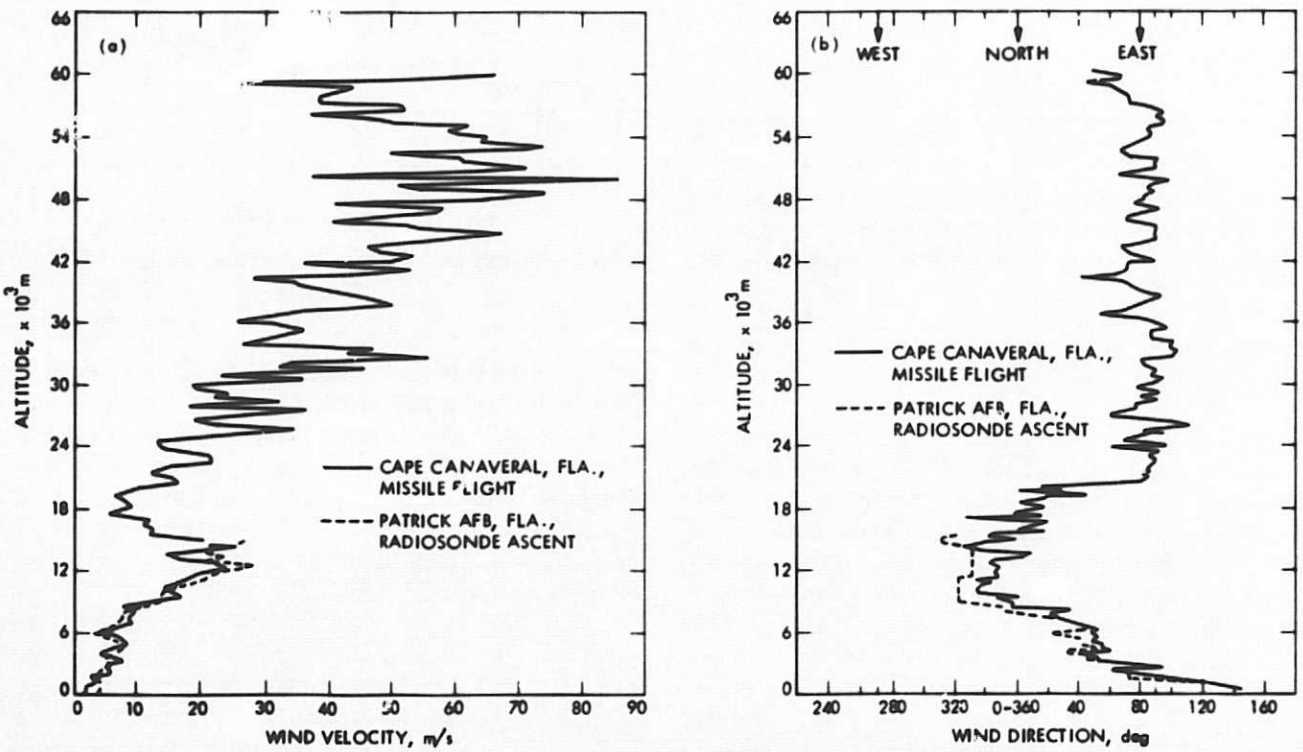

Fig. 4. Wind parameters according to altitude: (a) speed, (b) direction

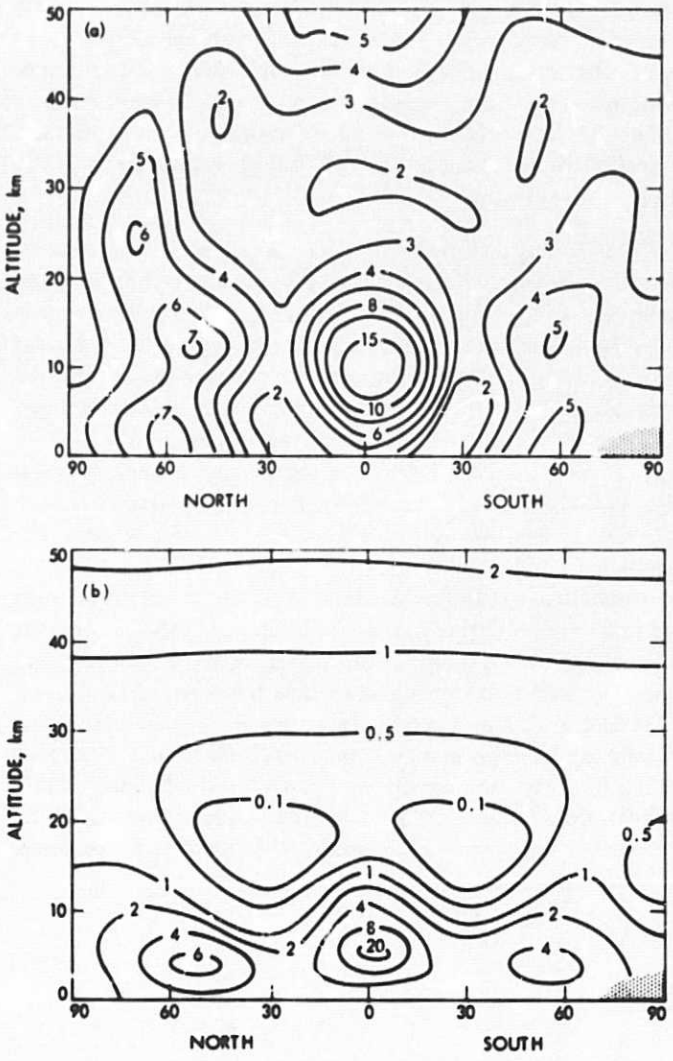

Fig. 5. The variation in values for transport coefficients with altitude and longitude for March through May: (a) horizontal (K_{yy}) distribution (10^4 cm^2 s^{-1}), (b) vertical (K_{zz}) distribution (10^4 cm^2 s^{-1})

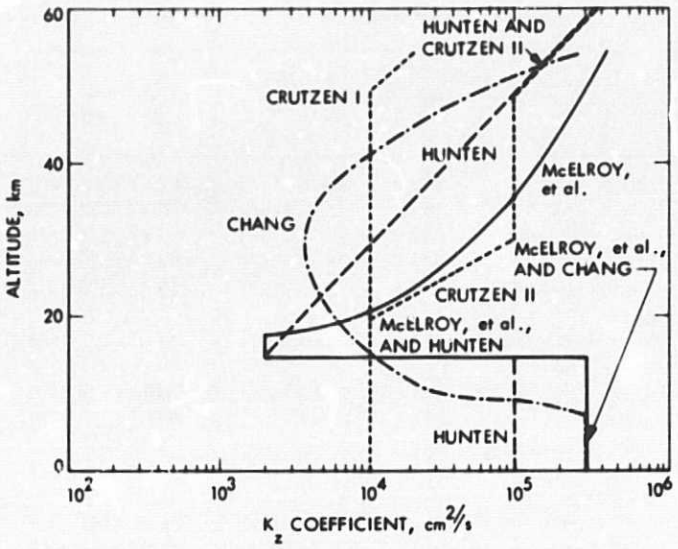

Fig. 6. K_z profiles used by different atmospheric modeling groups

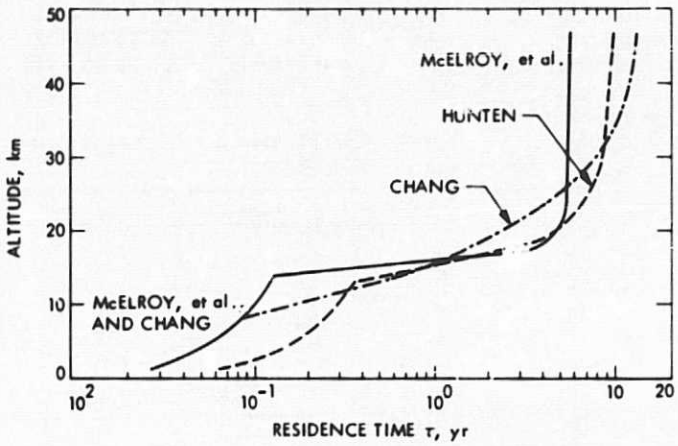

Fig. 7. Residence time profiles calculated using K_z coefficients from Fig. 6

among the modeling community is that the best K_z profile is similar to that used by McElroy, et al.

Figures 8 and 9 are graphs of the K_z profile and resultant residence times used by Yung (Ref. 14) in his model of the atmosphere. We used Yung's model to obtain the concentration profiles in Figs. 10 and 11. These profiles illustrate the decrease in concentrations and mean altitude of the pollutant following a 40-km and a 100-km injection. Based on this model, a pollutant injected at 100 km does not reside significantly longer in the atmosphere than for a 40-km injection. Since the eddy diffusion coefficients used in the Yung model are similar to those of McElroy, et al., both predict that the residence time is approximately constant above 25 km. It is probable that the model (Ref. 14) used to obtain the concentration profiles in Figs. 10 and 11 indicates a more rapid vertical dispersion than would be predicted by other models. While these differences are of academic interest, the resulting impacts calculated in this evaluation would not appreciably change if an alternate K_z profile were used. Figure 12 illustrates how the mixing ratio of a pollutant injected at 100 km decreases with time, due to vertical dispersion, and becomes more uniform with altitude.

Above 100 km, the total particle density decreases and molecular diffusion becomes the dominant mechanism for vertical mixing as illustrated in Fig. 13 (Ref. 15). The rate of dispersion in this region of the atmosphere can be described by the equation for spherically symmetric diffusion (Ref. 16):

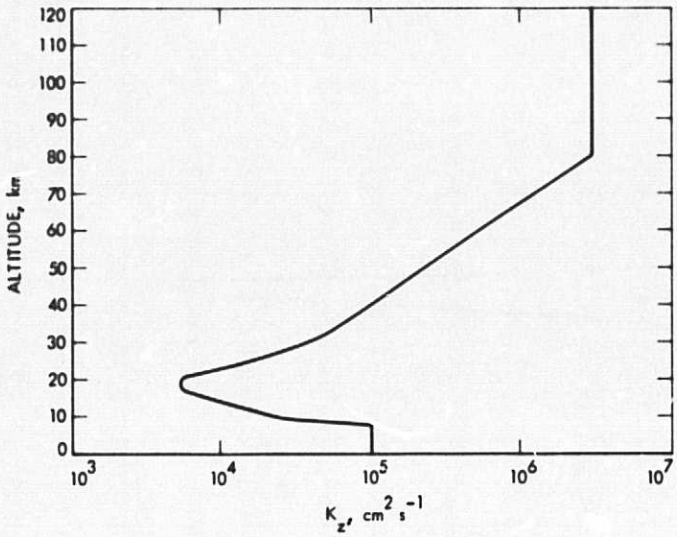

Fig. 8. K_z profile used in Yung's model

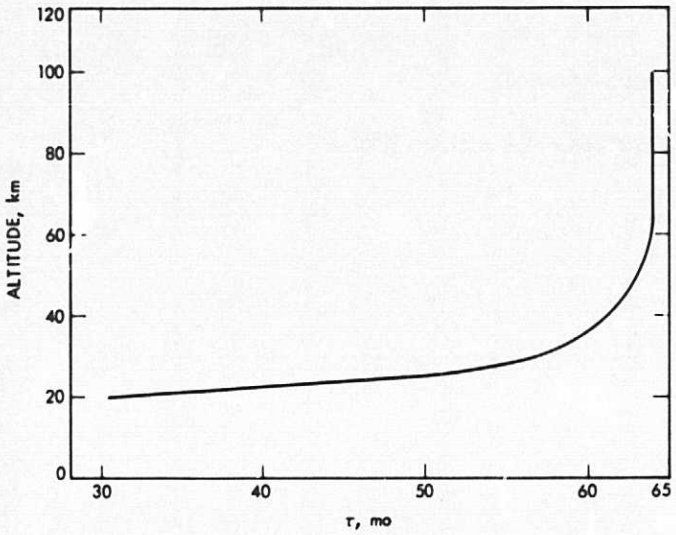

Fig. 9. Residence time profile calculated using K_z coefficients from Fig. 8

$$\frac{\partial n}{\partial t} = D^2 \nabla n = \frac{D}{r^2} \frac{\partial}{\partial r} \left(r^2 \frac{\partial n}{\partial r} \right)$$

$$= D \left[\frac{\partial^2 n}{\partial r^2} + \frac{2}{r} \frac{\partial n}{\partial r} \right]$$

where:

n = particle density

r = radius of the cloud

t = time

The solution can be written:

$$n(r, t) = \frac{S_o}{(4\pi Dt)^{3/2}} \exp(-r^2/4Dt)$$

where S_o is the total number of molecules injected and D is the molecular diffusion coefficient. This mathematical treatment of plume dispersion was not used in the present report because no propellant, or only a very small portion of the propellant, would be injected above 100 km.

C. Plume Dispersal in the Stratosphere

The first situation to be considered is that where the SS mission is aborted in the stratosphere. The propellant can be released in any 50-s, 100-s, or 200-s time period, while the SS is in the altitude range of 43 to 28.4 km. The trajectory of the SS during the injection mode and the duration of the dumping procedure determines the altitude regime of the injection. As the rate at which the plume disperses is predominantly a function of rapid horizontal mixing processes, the rate of plume expansion is enhanced by deposition over a wider altitude range.

Four different stratospheric propellant releases are considered; 50 s, 100 s, and 200 s releases initiated at 744 s GET (the earliest opportunity in Segment III), and a 50-s release initiated at 771 s GET. The releases initiated at 744 s correspond to an altitude of 43 km, and the 771-s release occurs at an altitude of 37.6 km. The release initiated at 771 s corresponds to the situation where the propellant is deposited in the narrowest possible regime, when the SS is on a near-horizontal flight trajectory.

Table 3 lists values for the critical parameters involved in the four cases: altitude regime, distance travelled by the SS during the ejection period, ejection duration, and initiation time (GET). In each of the cases, (a) through (d), the amounts of F_2 and N_2O_4 are 4.2×10^{28} and 2.2×10^{28} molecules. The N_2O_4 rapidly undergoes thermal decomposition resulting in the production of 4.4×10^{28} molecules of NO_2.

Although the diameter of the propellant exit port is postulated at only 2.5 cm, the plume diameter rapidly (less than one second) expands by a factor of 50 to 200 due to the pressure differential between the ejected plume and the ambient atmosphere. In case (a), the gas pressure in a 2.5-cm diameter plume would be ~8500 times the total pressure of the ambient atmosphere. In cases (a) and (d) the initial plume diameter would be ~4 to 5 m, whereas in cases (b) and (c) the plume diameters would be 2 to 2-1/2 and ~1 m respectively. Thus in cases (b) and (c) the plume does not expand as much, due

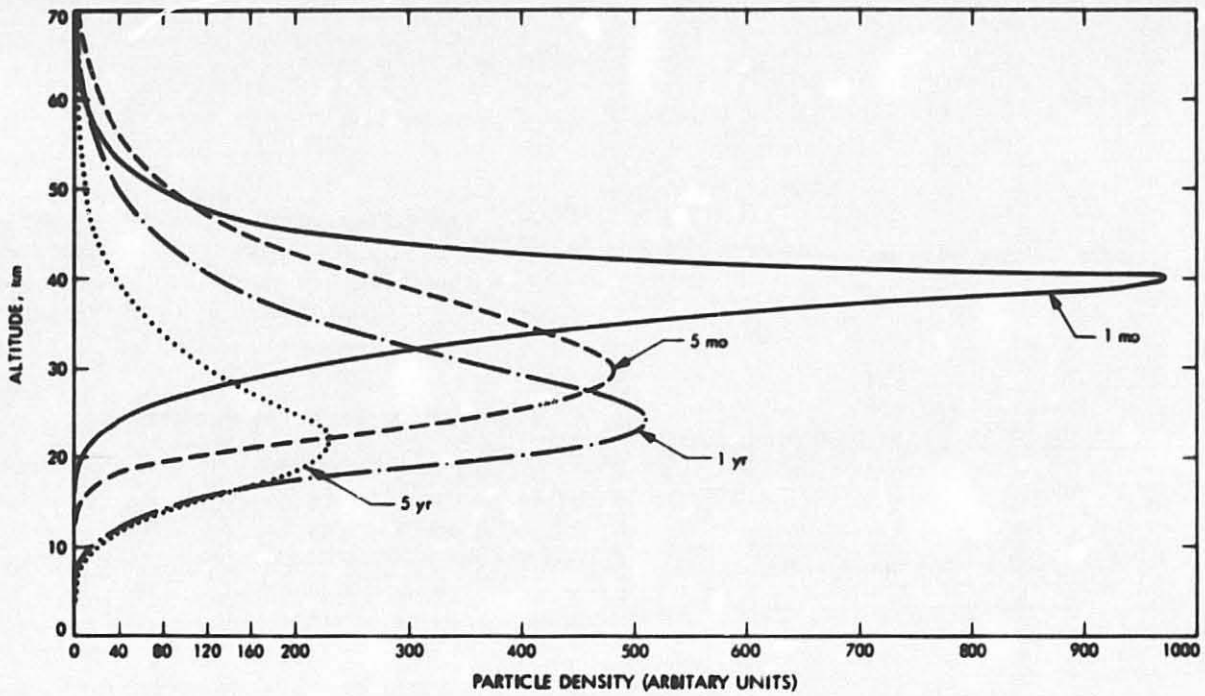

Fig. 10. Profiles of propellant concentrations following an injection at 40 km

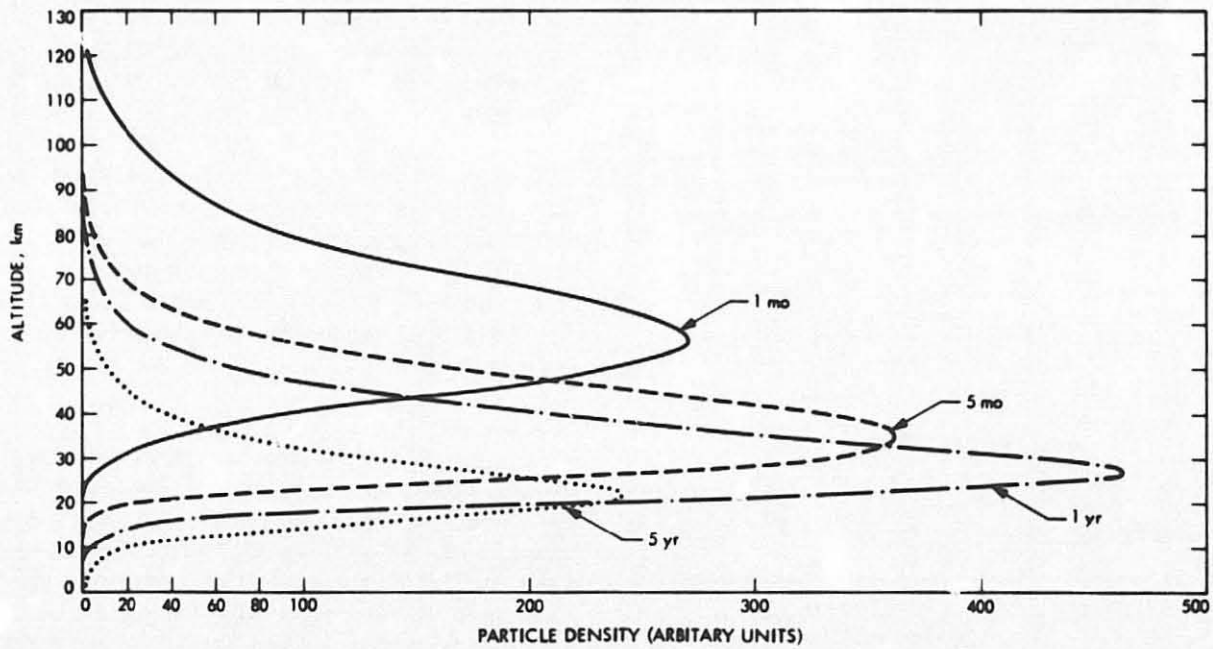

Fig. 11. Profiles of propellant concentrations following an injection at 100 km

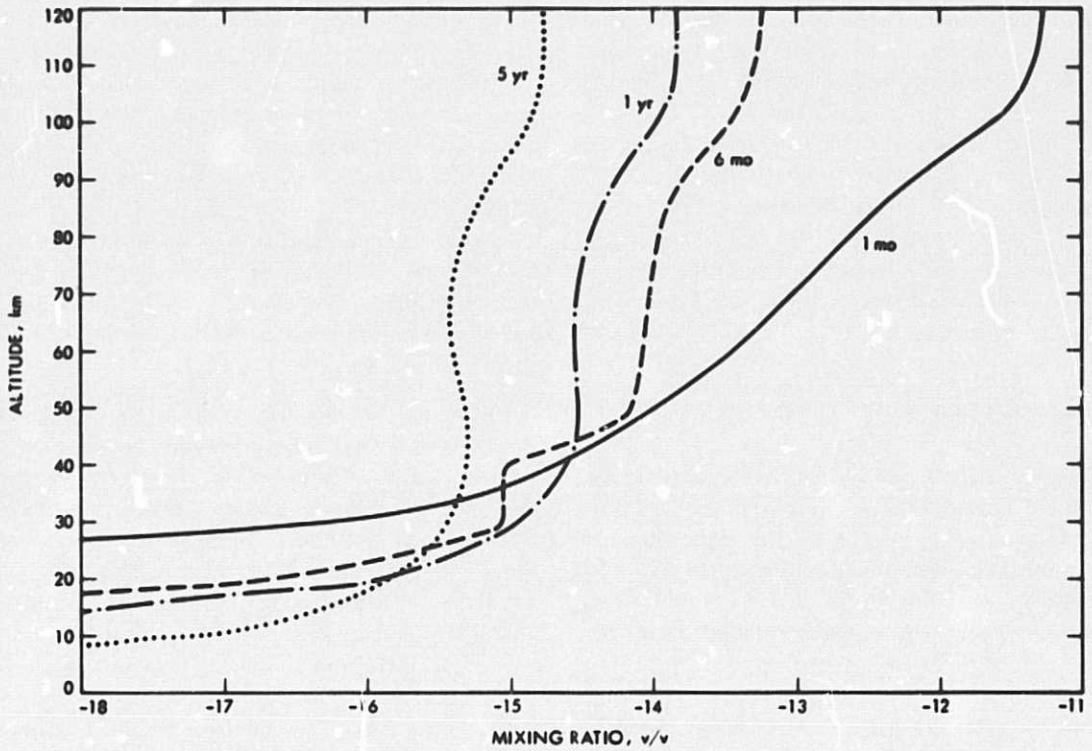

Fig. 12. Mixing ratio of the injectant at different altitudes as a function of time following an injection at 100 km

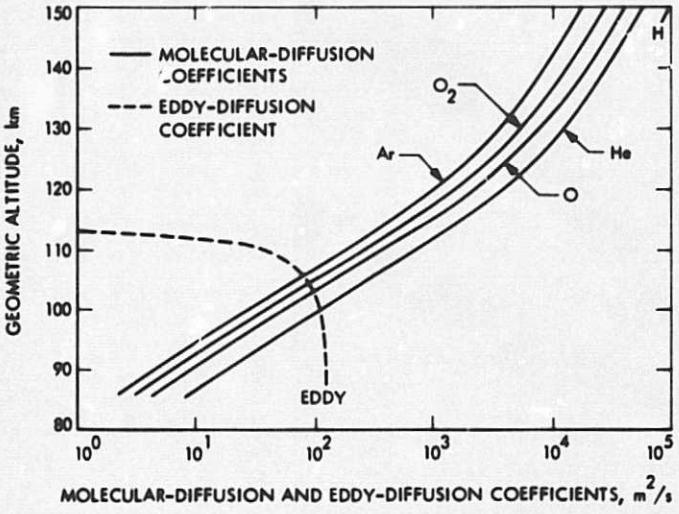

Fig. 13. Dominant mechanisms inducing plume dispersal according to altitude

to a lower pressure differential between the plume and the ambient atmosphere.

As soon as the gas is ejected into the atmosphere, it undergoes shearing by horizontal winds and dispersion due to turbulent diffusion. Figure 14 illustrates the horizontal and vertical mean "cloud" widths, and turbulent diffusion coefficients,

Table 3. Critical parameters for sample stratospheric injections

Case	Altitude, km	Duration, s	Distance, km	Initiation times
(a)	43.0 to 35.7	50	92.9	744
(b)	43.0 to 34.4	100	175.8	744
(c)	43.0 to 28.4	200	306.1	744
(d)	37.6 to 38.5	50	86.5	771

K_{yy}, K_{yz}, and K_{zz}, as a function of travel time (plume age) for a hypothetical point source injection (Ref. 17). It can be seen from this figure how the magnitude of K_{yy}, the horizontal eddy diffusion coefficient, varies with time (or plume diameter). At short times the dispersion is isotropic and approaches the molecular limit for the injection altitude, and then K_{yy} increases as $\sigma_h^{1.15}$ up to $\sigma_h \cong 100$ km (σ_h = horizontal dispersion cloud width), at which point it reaches the global limit. The global limit shown for K_{yy} in Fig. 14 corresponds to a value of $\sim 3 \times 10^{10}$ cm^2-s^{-1}, which is approximately an order of magnitude greater than the values calculated by Louis (Ref. 11), but comparable to those calculated by Crutzen (Ref. 18), in their two-dimensional models. The values of K_{yy} calculated by Louis and Crutzen were typically 3×10^9 cm^2-s^{-1}, and $> 10^{10}$ cm^2-s^{-1} respectively, and represented meridional dispersion (N-S). Zonal dispersion is prob-

ably comparable in magnitude. Although Fig. 14 has been used to estimate the rate of horizontal dispersion, it has been realized that the data base used to develop this figure is limited at best. If Fig. 14 is in error at short times ($t < 10^5$ s), it would probably be on the side of underestimating the rate of plume dispersal due to an incorrect time evolution for K_{yy}. However, at longer times, Fig. 14 may overestimate the rate of dispersal if the global asymptotic value for K_{yy} is too high. For the region where K_{yy} or K_{zz} have reached their asymptotic values, the rate of plume dispersal can be calculated using the following simpie expression:

$$\sigma^2 \text{ (mean plume width)}^2 = 4\,K\,t$$

Figure 14 has been used in this assessment to calculate the time history of the plume volume. In this figure and our subsequent calculations, K_{yy} represents the parameterized eddy diffusion coefficient which describes both small and large scale eddies. *It can be seen from Fig. 14 that the plume size at long times is independent of any assumptions made about the initial shape and size of the plume.* Whether the initial cloud width is 1, 10, or 100 m, it will still expand to ~10^2 km after 1 day and ~10^3 km after 10 days. Consequently, the estimated plume width after 1 day, 1 month, and 1 year were taken directly from Fig. 14. At short times (< 1 day) the calculated plume volumes may be somewhat dependent upon the validity of various approximations. As stated earlier, the initial diameter of the gas plume (within a few seconds after release) is dependent upon the ratio of the "plume pressure" and the ambient pressure of the atmosphere. The plume will rapidly expand to eliminate the pressure gradient. In addition, as the SS takes either 50, 100, or 200 s to release its propellant, the gas released at the beginning of the period has more time to disperse. Consequently, the shape of the plume at the end of the period can best be described as the tilted frustrum of an inverted cone (see Fig. 15a).

Although the SS travels ~93 km during this period, it descends only ~7.3 km in altitude, largely confining the propellant to this altitude regime for several months due to the slow rate of vertical mixing. *Consequently the plume is predicted to expand rapidly in volume by horizontal dispersion, but only very slowly by vertical mixing.* This merely reflects the large difference in magnitudes between the rates of horizontal and vertical mixing. Within a few days, the shape of the plume changes from the tilted frustrum of a cone (shown in Fig. 15a) to that of a cylinder illustrated in Fig. 15b. For times between the end of the dumping period and the time it takes for the plume to reach the shape of a cylinder, the plume

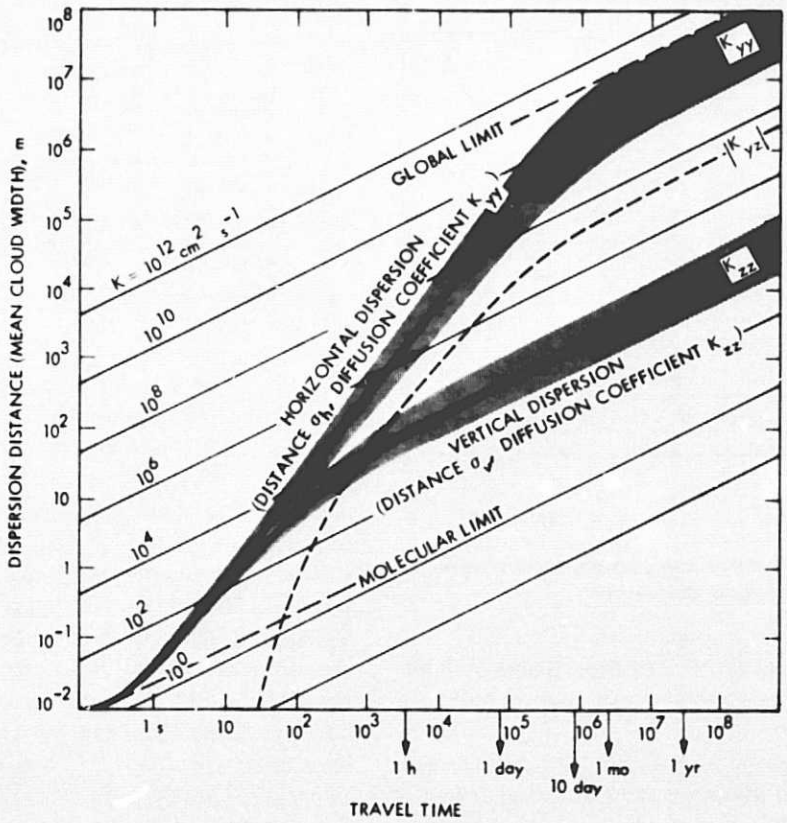

Fig. 14. Dispersion distances and coefficients of turbulent diffusion as a function of time following an injection at 100 km

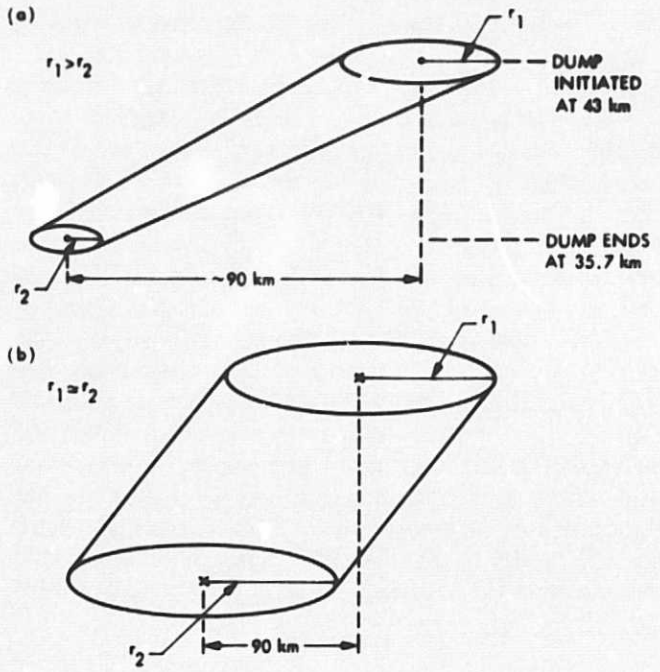

Fig. 15. Geometric shape of the propellant plume: (a) initial shape of plume, (b) plume shape after a few days

shape and rate of expansion are less easily calculated. However, it is quite adequate and intuitively correct to assume that the shape of the plume can be described, for the purpose of calculating its rate of expansion, by a cylinder ~7.3 km in height with an initial volume equivalent to that of the initial tilted inverted cone.

These calculations of plume volume are probably good to within only an order of magnitude because of uncertainty in K_{yy}. The plume dispersal rates will vary greatly depending upon the meteorological conditions prevailing at the time. K_{yy} is predicted to exhibit significant variability with both latitude and season (Ref. 11). Table 4 shows the calculated plume volumes and resultant FX and NO_x concentrations and mixing ratios as a function of time, assuming no vertical mixing. This approach is obviously invalid at times greater than 1 month and leads to a small underestimate of the true plume volume.

D. Plume Dispersal in the Mesosphere

The propellant can be released during any 50-, 100-, or 200-s time period while the Space Shuttle ascends from 62.2 km to 125.9 km (152.9 – 362.9 s GET), or descends from 91.4 km to 70.0 km (442 – 654 s GET). Any 50-s dump in flight Segment I will initially be distributed within an atmospheric layer 15 km in height, and over a horizontal distance of ~79 km. The initial volume of the plume (at the end of the dump period) is governed by the almost instantaneous expansion that occurs due to the pressure differential between the ejected propellant and the ambient atmosphere (the initial expansion is greatest at higher altitudes due to the lower atmospheric pressure). Let us consider two extreme cases: (1) a 50-s dump between 62 and 77 km, and (2) a 50-s dump between 111 and 126 km. It is easily shown that the initial diameter of the propellant plume will be ~42 m in case (1) and 2.54 km in case (2). From Fig. 14, it can be seen that there will be no significant expansion of the plume within the dump period due to eddy processes. (This is in contrast to the stratospheric case.) The initial plume volumes are 3×10^{13}

Table 4. Time history of plume volumes and concentrations of FX and NO_x for a stratospheric injection

Time	Plume volume, cm^3	Cloud width, km	[FX][a], molecules/cm^3	[NO_x], molecules/cm^3	(FX)[b] mixing ratio	(NO_x)[b] mixing ratio
0	3.2×10^{12}	2.4×10^{-2}	1.34×10^{16}	1.38×10^{16}	0.17	0.17
1 h	1.0×10^{16}	1.4×10^{0}	5.0×10^{12}	4.4×10^{12}	6.3×10^{-5}	5.5×10^{-5}
5.6 h	1.0×10^{18}	1.4×10^{1}	7.1×10^{10}	4.4×10^{10}	8.9×10^{-7}	5.5×10^{-7}
1 day	5.1×10^{19}	9.6×10^{1}	1.66×10^{9}	8.6×10^{8}	2.1×10^{-8}	1.1×10^{-8}
10 days	8.7×10^{21}	1.26×10^{3}	9.8×10^{6}	5.1×10^{6}	1.2×10^{-10}	6.4×10^{-11}
1 mo	7.4×10^{22}	3.7×10^{3}	1.16×10^{6}	5.9×10^{5}	1.4×10^{-11}	7.4×10^{-12}
1 year	1.8×10^{24}	Hemisperic	4.7×10^{4}	2.5×10^{4}	5.9×10^{-13}	3.1×10^{-13}
5 years	3.6×10^{24}	Global	2.3×10^{4}	1.25×10^{4}	2.9×10^{-13}	1.6×10^{-13}

[a] $FX = HF + F + FO + FO_2 + HOF + NOF$

[b] It is assumed that the cloud center remains at 40 km, there is no vertical dispersion, and the propellant is uniformly mixed within the cloud. Both assumptions are incorrect, but are used for simplicity (discussed with reference to Fig. 11). $[M] = 8.0 \times 10^{16}$ molecule-cm^{-3} (total gas content at 40 km). At times less than one day, the values shown for FX have taken into account the F_2 photo dissociation rate (each molecule of F_2 produces 2 FX molecules).

cm^3 and 2×10^{16} cm^3 respectively. The plume width at times longer than several hours is not dependent upon the initial size of the plume (Fig. 14). Consequently, the time history of the cloud width will be the same for any dumping altitude or dump duration. The volume is dependent on the dump duration as this governs the initial height of the plume. Table 5 shows the predicted time history of the plume width, plume volume, [FX], and [NO_x].

Table 5. Plume volumes and concentrations of FX and NO_x for an injection in the ionosphere

Time	Plume width, km	Plume volume, cm^3	[FX]	[NO_x]
1 h	2	4.7×10^{16}	1.8×10^{12}	9.4×10^{11}
1 day	96	1.1×10^{21}	7.8×10^{7}	4.0×10^{7}
10 days	1.26×10^{3}	1.9×10^{22}	4.6×10^{6}	2.3×10^{6}
1 mo	3.7×10^{3}	1.6×10^{23}	5.4×10^{5}	2.8×10^{5}
1 year	Hemispheric	3.9×10^{24}	2.2×10^{4}	1.1×10^{4}

From these values of plume volume and [FX] (it has been assumed 2 FX molecules are produced per F_2 injected), the mixing ratios (v/v) of FX at different injection altitudes were calculated (Table 6). When the propellant is released over a 100- or 200-s time period, these values must be reduced by factors of 2 and 4 respectively. In addition, these values neglect vertical dispersion, which is quite significant at times greater than 1 month at these high altitudes. Figures 11 and 12 show how vertical plume dispersion is quite rapid for high altitude injections. Therefore these values tend to overestimate the mixing ratios of FX and NO_x (almost identical to FX – see Table 5).

Table 6. The mixing ratios (v/v) of FX at different altitudes following an ionospheric injection

Time	70 km	90 km	120 km
1 day	3.9×10^{-8}	1.0×10^{-6}	1.4×10^{-4}
10 days	2.3×10^{-9}	6.0×10^{-8}	8.5×10^{-6}
1 mo	2.7×10^{-10}	7.0×10^{-9}	1.0×10^{-6}
1 year	1.1×10^{-11}	3.0×10^{-10}	4.1×10^{-8}

III. Atmospheric Modeling

A. Background

Basically, a stratospheric model is a set of equations representing all constant and dynamic aspects of the stratosphere that have a direct or indirect effect on the concentrations of the relevant chemical species. Representative mathematical expressions are used to generate a computer program. These models have become increasingly complex, to the point that a run may take hours or days of computer time. Typically, a model takes years to develop and will require the concentrations of thirty chemical species while utilizing rate constants, k and J values (for photochemical reactions), for 100 or more reactions. Additionally, the models must take into account natural variations in background levels, diurnal variations of sunlight, the horizontal and vertical movements in the stratosphere, and the altitude and location of the pollutant injection. Finally, many of the concentrations, rate constants, and other input data are unavailable and must be estimated. Thus, it is easy to see that two groups of modelers could make different estimates and predict different outcomes. In fact, most recently, not only the magnitude, but also the sign of the impact of the SSTs is in dispute. Some groups presently claim that SSTs flying at 17 km would increase rather than decrease the level of stratospheric zone (Ref. 19)

Models exhibit varying levels of sophistication or "parameterization" according to the level of data-averaging that is involved. The least complex models are 1-D (dimension) models, or vertical profiles. These models emphasize completeness with regard to the chemistry of the stratosphere and are very comprehensive with regard to the reactions in the model. Vertical transport is also emphasized. However, horizontal movement, on a micro or macro level, is ignored and 1-D models must assume a globally-averaged input. Additionally, vertical transport as well as the ambient concentrations must be averaged to account for geographical variations. Thus, the 1-D model cannot predict the extent of local or "corridor" perturbations (disruptions) in the stratospheric chemistry because the output is only a vertical profile. However, the 1-D models use a fine vertical grid size, thereby allowing for more detail in the vertical direction. They also allow for more completeness with regard to photochemistry.

The 2-D models represent a cross-section of the stratosphere through a polar axis. While 2-D models can incorporate more detail for K_{yy} (the zonally averaged meridional eddy diffusion coefficient representing north-south horizontal transport), often fewer reactions are included and the vertical grid size may be larger. This addition of K_{yy} is a substantial addition in that interhemispheric transport is relatively slow and the altitude of the ozone layer exhibits variation according to latitude.

Finally, there are 3-D models. These models make maximum use of horizontal diffusion in both the polar and equatorial (K_x) directions. However, still more detail in the chemistry and subdivision of the stratospheric layer must be

sacrificed. Furthermore, the demand for computer time to run the model substantially increases.

B. Assessing an NO_x Injection

The model for NO_x injections has undergone intensive development under the Climatic Impact Assessment Program (CIAP), Department of Transportation. Under CIAP, several models have been developed to predict the impacts of present subsonic and future levels of SST flight on the stratosphere. Thus, the NO_x models are well established and, while some areas of controversy still remain over effects of aircraft injections at lower stratospheric levels, the models are in substantial agreement regarding the overall role of NO_x. (The agreement between 1-, 2-, and 3-D models is not unexpected in that, although lower-order models use averaged data for more of the parameters, the data base itself is the same for all of the models.)

In this assessment we have taken advantage of the advanced state of NO_x models. In so doing, we have used the results from existing models to predict the ozone perturbation, at steady state (equilibrium) conditions, expected to result from an NO_x injection from the SS payload. This analysis is presented in Section IV.

C. Assessing an FO_x Injection

In the course of assessing the impacts of the HCl injected into the stratosphere by the SS main engines (not to be confused with the present case of a SS payload propellant), models were developed for stratospheric chlorine chemistry. From that HCl assessment, the catalytic nature of chlorine destruction of ozone was realized, even though the HCl injected by the main engines appeared not to pose a serious threat to the ozone layer (worst case predictions are ~0.5% decrease in ozone) (Ref. 6), Rowland and Molina (Ref. 20) did a study indicating that chlorofluoromethanes (CFMs) can photodissociate in the upper stratosphere generating Cl, but not in the troposphere. This causes long atmospheric lifetimes for the CFMs (to date no tropospheric chemical sinks have been identified), allowing long-term stratospheric accumulation of Cl. Due to the tremendous quantities of CFMs used as aerosol propellants, CFMs were realized as a potentially very substantial threat to the ozone layer. Hence, much like NO_x, models have been developed for stratospheric ClO_x chemistry and for stratospheric injections of Cl. These ClO_x models are also well established. While controversies remain over details of the models, the predictions of the various ClO_x models are substantially the same (Ref. 21).

Although chlorine and fluorine are different substances, they are of the same family, i.e., halogens, and exhibit very similar chemistries. In assessing the impacts of the fluorine injection, we have taken advantage of the advanced state of ClO_x models as well as the analogous qualities of Cl and F chemistries.

It is not realistic to merely substitute the value for the fluorine injection into a chlorine model. Rather, stratospheric fluorine chemistry has been very carefully analyzed to generate analytic expressions for the catalytic efficiency of fluorine comparable to those of Cl. Using experimental and estimated rate constant data, the ratio of the values for the F and Cl catalytic efficiencies has been calculated. This factor is then used to convert the ozone perturbation predicted for a chlorine injection in a ClO_x model to that predicted for a FO_x injection of the same magnitude. Thus, the full benefit of a sophisticated stratospheric model can be realized in determining the ozone perturbation resulting from the fluorine injection.

Details regarding analytic expressions, rate constant data, and the fluorine model, as well as the actual quantities calculated and overall assessment, are presented in Section V.

IV. N_2O_4 in the Atmosphere

A. Background

An NO_x model has been developed for high flying aircraft and is fairly well established. Figure 16 is a schematic diagram of the chemistry used in the NO_x model. The principal chemical reactions incorporated into the NO_x model are summarized in Table 7.

Although the pollutant is injected in the form of N_2O_4, reaction (18),

$$N_2O_4 + M \rightarrow 2NO_2 + M \qquad (18)$$

is very rapid under stratospheric conditions and the entire amount will dissociate within 1 to 2 seconds to form NO_2. Therefore, for purposes of analysis, the dumping can be considered an NO_2 injection, the form similar to aircraft exhaust. Furthermore, since NO and NO_2 cause the catalytic destruction of ozone through reactions (11) and (12), they are both considered to be in the "active" partition and are collectively termed NO_x. The basic mechanism for production of ozone in the stratosphere is as follows (Chapman mechanism):

$$O_2 + h\nu \rightarrow O + O \qquad (1)$$

$$O + O_2 + M \rightarrow O_3 + M, \text{ twice} \qquad (2)$$

Net: $3O_2 + h\nu \rightarrow O_3 + O_2$

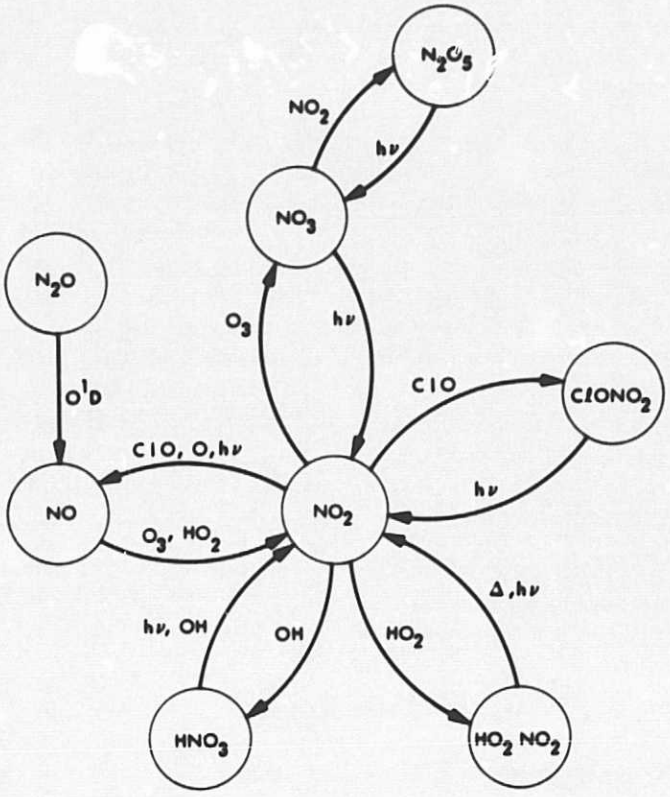

Fig. 16. Schematic diagram of the NO_x stratospheric model

Table 7. Stratospheric NO_x model

Reaction		Equation No.
$O_2 + h\nu$	$\rightarrow O + O$	(1)
$O + O_2 + M$	$\rightarrow O_3 + M$	(2)
$O_3 + O$	$\rightarrow O_2 + O_2$	(3)
$O_3 + h\nu$	$\rightarrow O_2 + O$	(4)
$O(^1D) + H_2O$	$\rightarrow HO + HO$	(5)
$HO + O_3$	$\rightarrow HOO + O_2$	(6)
$HOO + O_3$	$\rightarrow HO + O_2 + O_2$	(7)
$HO + O$	$\rightarrow H + O_2$	(8)
$HOO + O$	$\rightarrow HO + O_2$	(9)
$H + O_3$	$\rightarrow HO + O_2$	(10)
$NO + O_3$	$\rightarrow NO_2 + O_2$	(11)
$NO_2 + O$	$\rightarrow NO + O_2$	(12)
$NO_2 + h\nu$	$\rightarrow NO + O$	(13)
$HO + NO_2 + M$	$\rightarrow HNO_3 + M$	(14)
$HNO_3 + h\nu$	$\rightarrow HO + NO_2$	(15)
$HOO + NO$	$\rightarrow HO + NO_2$	(16)
$NO_2 + O_3$	$\rightarrow NO_3 + O_2$	(17)

This reaction set produces ozone in the stratosphere at a total rate of about 5.0×10^{31} molecules/s (Ref. 22).

In a pure oxygen system, ozone is destroyed by reaction (3).

$$O_3 + O \rightarrow O_2 + O_2 \qquad (3)$$

Although ozone can be rapidly photolyzed (4), this does not result in the loss of ozone as reaction (4) is usually followed by (2)

$$O_3 + h\nu \rightarrow O_2 + O \qquad (4)$$

$$O + O_2 + M \rightarrow O_3 + M \qquad (2)$$

Net: null reaction

Hence, the rate of ozone destruction is a function of the relative rates of (3) and (2) with respect to [O]. This net cycle (4 followed by 2) is important in controlling the temperature stability of the stratosphere due to the exothermicity of reaction (2).

The HO_x family provides additional reaction-pairs that cause the catalytic destruction of ozone; three examples are shown (6)–(7), (6)–(9), and (10)–(8).

$$HO + O_3 \rightarrow HOO + O_2 \qquad (6)$$

$$HOO + O_3 \rightarrow HO + O_2 + O_2 \qquad (7)$$

Net: $2\,O_3 \rightarrow 3\,O_2$

$$HO + O_3 \rightarrow HOO + O_2 \qquad (6)$$

$$HOO + O \rightarrow HO + O_2 \qquad (9)$$

Net: $O_3 + O \rightarrow O_2 + O_2$

$$H + O_3 \rightarrow HO + O_2 \qquad (10)$$

$$HO + O \rightarrow H + O_2 \qquad (8)$$

Net: $O_3 + O \rightarrow O_2 + O_2$

However, these three cycles must compete for HO_x with a net zero balance cycle.

$$HO + O_3 \rightarrow HOO + O_2 \quad (6)$$

$$HOO + NO \rightarrow HO + NO_2 \quad (16)$$

$$NO_2 + h\nu \rightarrow NO + O \quad (13)$$

$$O + O_2 + M \rightarrow O_3 + M \quad (2)$$

Net: null reaction

A comparable catalytic destruction cycle and competing neutral cycle are demonstrable for NO_x chemistry.

$$NO + O_3 \rightarrow NO_2 + O_2 \quad (11)$$

$$NO_2 + O \rightarrow NO + O_2 \quad (12)$$

Net: $O_3 + O \rightarrow O_2 + O_2$

$$NO + O_3 \rightarrow NO_2 + O_2 \quad (11)$$

$$NO_2 + h\nu \rightarrow NO + O \quad (13)$$

$$O + O_2 + M \rightarrow O_3 + M \quad (2)$$

Net: null reaction

Thus for these NO_x cycles the relative rates of reactions (12) and (13) determine how much ozone will be destroyed.

B. NO_x Modeling

As is the case with any body of knowledge, NO_x models have evolved through a series of changes to reach their present form, and continue to evolve as values for rate constants and transport coefficients are improved, and as new reactions are added to the models. Table 8 and Fig. 17 summarize the evolution of the predicted change in stratospheric ozone in response to new or improved rate constant data and addition of new reactions to the model. It is evident that the most recent change, the new rate constant for reaction (16),

$$HOO + NO \rightarrow HO + NO_2 \quad (16)$$

Table 8. Summary of changes in predicted ozone levels for the stratospheric NO_x model

Change made	Computed ozone reduction, %	
	17 km	20 km
Start (1974)	4.8	~11
New Chang (Ref. 23) eddy diffusion	5.4	12
($N_2O + h\nu$) changed from Bates and Hayes to (Ref. 24) Johnston and Selwyn (Ref. 25)	5.3	12
Add "smog" reactions: OH + CO, $O + CH_4$, $H_2O_2 + O$, $HO_2 + h\nu$, $OH + CH_4$	4.8	11
$OH + HO_2$ ($2 \times 10^{-10} \rightarrow 2 \times 10^{-11}$)	2.1	6.4
$OH + HNO_3$ ($1.3 \times 10^{-13} \rightarrow 8.9 \times 10^{-14}$)	2.0	6.0
$NO_3 + h\nu$ (branching, $NO + O_2 \rightarrow$ 2/3 ($NO_2 + O$), 1/3 ($NO + O_2$))	1.6	5.2
$O(^1D)$ reactions with N_2O, N_2, O_2, CH_4, H_2O changed from Hampson and Garvin (Ref. 26) recommendations to Streit et al., (Ref. 27) recommendations	1.5	4.9
$OH + NO_2 + M$ (Tsang (Ref. 28) → Anastasi (Ref. 29) et al.)	1.5	4.8
$HO_2 + HO_2$ (3×10^{-11} exp (-500/T) → 1.7×10^{-11} exp (-500/T))	1.2	4.3
$HO_2 + O$ (8×10^{-11} exp (-500/T) → 3×10^{-11}))	1.2	4.2
$HO_2 + NO$ (Howard and Evenson, Ref. 30)	+1.9[a]	+.4[a]

[a]Ozone increase.

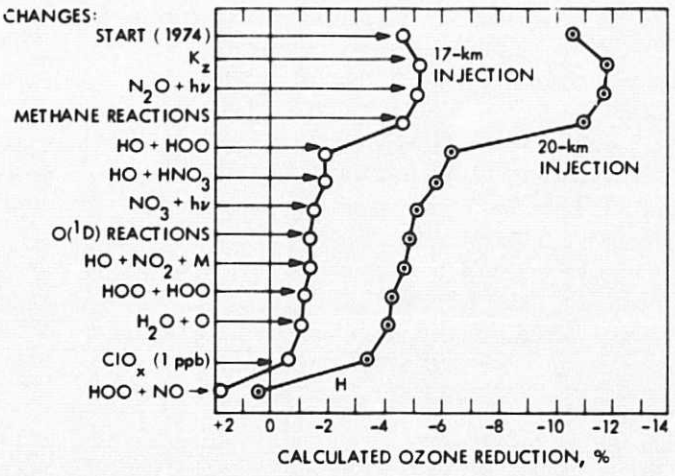

Fig. 17. Evolution of the predicted change in stratospheric ozone from stratospheric SST flight.

has changed not only the magnitude, but also the direction of the ozone perturbation for 17- and 20-km injections; i.e., the models now predict an increase in the integrated ozone column rather than a decrease (Ref. 31).

Another recent development in modeling theory was an uncertainty analysis whereby an attempt was made to quantitate variability in the models that is due to uncertainties in the available rate-constant data. In such an analysis, Stolarski, et al., (Ref. 32) assigned a normal (Gaussian) distribution to the levels of uncertainty for reaction rate constants. Performing several hundred model runs while individually varying rates for each of the 48 reactions used in their model, they concluded that a reduction of all rate measurement uncertainties to ±15% would result in an overall uncertainty of ±30% for a given calculation of ozone reduction. They suggest, however, that a factor of two is a realistic estimate of uncertainty for results from present models. However, this type of model is in its infancy, and it is dubious whether the data base for the reaction rate constants is adequate at present. In addition, the more fundamental question to be answered is whether a 1-D model is adequate for an ozone perturbation calculation.

The quality of the models is expected to improve with changes in the data base. In fact, several of the gaps which need to be filled were discussed in a recent review of stratospheric modeling with regard to aircraft (Ref. 31). Some of the more prominent items are simultaneous measurements of individual species to validate certain aspects of the 1-D photochemical models, instruments to accurately measure water vapor in the stratosphere, and improvements in modeling techniques to account for the true (nonlinear) nature of the atmosphere.

C. Impact of the Stratospheric NO_x Injection

The impact of the NO_x injection on the stratosphere was calculated, in terms of $-\Delta O_3$, by two methods. From a 2-D model created by the Lawrence Livermore Laboratory (Ref. 33), the result for an SST fleet flying at an altitude of 35 km was linearly scaled down to an injection magnitude of one SS abort flight per year. The second approach used was based on a formula from Johnston (Ref. 34), for $\Delta O_3/\Delta NO_x$ following a 20-km injection; $-\Delta O_3/O_3 = (1/5)\ \Delta NO_x/NO_x$. The result from this latter approach is less reliable due to numerous changes in rate constant data since the formula was derived, and due to differences in injection altitude.

LLL 2-D Model (Ref. 33)

SST Fleet:

Injection = 3.2×10^{34} molecules yr^{-1}

$\Delta O_3 = -17.24\%$

SS Injection:

Injection[1] = 4.6×10^{28} molecules NO_2

$$\Delta O_3 = \frac{4.6 \times 10^{28}}{3.2 \times 10^{34}} (-17.24\%)$$

$$\Delta O_3 = -2.48 \times 10^{-5}\%$$

Johnson Correlation (Ref. 27)

$$\frac{\Delta O_3}{O_3} = \frac{1}{5} \frac{\Delta NO_x{}^2}{NO_x}$$

$$\frac{\Delta O_3}{2 \times 10^{12}} = \frac{1}{5} \frac{\Delta NO_x}{2 \times 10^{9}}$$

$$\Delta O_3 = \frac{1}{5} \frac{(4.6 \times 10^{28}) \div (7.08 \times 10^{36}) \times (2 \times 10^{12})}{2 \times 10^{9}}$$

$$= -2.6 \times 10^{6} \text{ molecules}$$

$$= -1.3 \times 10^{-4}\%$$

The $-\Delta O_3$ calculated is $\sim 5 \times 10^5$ (SST model) to $\sim 3 \times 10^6$ molecules cm^{-3}-s^{-1}. This represents a change of $\sim 10^{-5}$ to 10^{-4}%. This constitutes a change in $[O_3]$ in the stratosphere about 4 orders of magnitude *less* than a change that would be detectable (~0.1%) (Ref. 6). Thus, for all practical purposes, it can be said that there are no impacts on stratospheric ozone from such a propellant dumping. This is not unexpected when one considers that existing SSTs emit an equal amount of NO_2 in less than 10 hours of cruise flight time.

D. NO_x Plume Chemistry in the Stratosphere

The release of N_2O_4 into the stratosphere is equivalent to the release of twice the quantity of NO_2 as the N_2O_4 will rapidly (in seconds) undergo thermal decomposition:

$$N_2O_4 \rightarrow NO_2 + NO_2$$

[1] Assuming one abort per year with the N_2O_4 propellant

[2] For one aborted mission.

The NO_2 thus produced will be photolyzed ($J \sim 10^{-2} s^{-1}$) within a few minutes to form an equal concentration of nitric oxide and atomic oxygen. The nitric oxide reacts with ozone to regenerate NO_2 while the atomic oxygen recombines with the large concentration of molecular oxygen to form ozone. The overall result is that NO and NO_2 rapidly attain a transitory steady-state equilibrium, which is accompanied by a net production of ozone.

$$N_2O_4 \rightarrow 2NO_2$$

$$NO_2 + h\nu \rightarrow NO + O$$

$$O + O_2 + M \rightarrow O_3 + M$$

$$NO + O_3 \rightarrow NO_2 + O_2$$

After this initial production of ozone, the standard NO_x catalyzed decomposition of odd oxygen occurs. This decreases the odd oxygen content within the plume. However, this perturbation will be highly localized and its impact on the total column abundance of ozone insignificant. Crutzen (Ref. 18) used a 2-D model to demonstrate that the observed O_3 perturbation that followed the injection of NO_x, via a solar proton effect, in the upper stratosphere/lower mesosphere could be adequately explained, thus lending some credence to our understanding of upper atmospheric ozone chemistry.

While the concentration of NO_x remains high relative to the normal ambient levels, the concentrations of numerous radicals deviate from their normal photochemically controlled equilibrium concentrations; e.g., the $OH(^2\pi)$: HO_2 ratio will be controlled by the $NO + HO_2$ reaction rather than the $O + OH$, and $O + HO_2$ reactions. However, these short-term perturbations are of little significance as the NO_x plume rapidly disperses, and normal photochemical equilibrium is rapidly reestablished.

E. Neutral Chemistry for a High-Altitude Injection of NO_x

Two of the three abort segments discussed in Section II occur in the altitude region of about 50 to 120 km, well above the stratosphere, encompassing the mesopheric and thermospheric regions of the atmosphere. As discussed in connection with plume dispersal, this material will be carried downward into the stratosphere at a rate that is relatively rapid, depending on the exact choice of eddy diffusion coefficients used for the calculation. *Following this mixing process, the effects in the stratosphere on the ozone layer will then be identical in character, though not in magnitude, to those previously discussed for the case of a direct injection into the stratosphere.* There are, however, certain effects of the high-altitude neutral chemistry that are of interest. One of these processes will have the effect of destroying significant fractions of the injected NO_x so that much of it will reach the stratosphere in an unreactive form.

We first review the sequence of events following the release of N_2O_4 in the high-altitude region. By far the most dominant mechanism for N_2O_4 destruction would be collisional dissociation, as previously concluded in the section on stratospheric effects:

$$N_2O_4 + M \rightarrow 2NO_2 + M \qquad (18)$$

The rate constant for this reaction is $4 \times 10^{-7} \exp(-5560/T)$ cm^3/s, so that for a total particle (M) density of 10^{15} cm^{-3} and a temperature of 220 K (which are typical for 80-km altitude), dissociation of the entire amount will occur in approximately four minutes. In all probability, this process will be accelerated somewhat by photodissociation,

$$N_2O_4 + h\nu \rightarrow 2NO_2 \qquad (19)$$

with a J-value that we estimate to be of the order of $10^{-3} s^{-1}$.

Similarly, the photodissociation of NO_2,

$$NO_2 + h\nu \rightarrow NO + O \qquad (13)$$

which occurs with a J-value of 10^{-2} s^{-1}, will dissociate the NO_2 in about two minutes. The reaction

$$O + NO_2 \rightarrow NO + O_2 \qquad (12)$$

will be even faster than the photodissociation, owing to the high concentrations of atomic oxygen (10^{10} to 10^{11} cm^{-3}) at the higher altitudes, combined with the very rapid rate constant for that reaction (9.1×10^{-12} cm^3/s).

The preceding discussion shows that the N_2O_4 *will be converted to* NO *on a time scale of minutes.* Coincident with the process of plume dispersal, as discussed in Section II, the NO will participate in several neutral chemistry reactions (in addition to those previously described), the main features of which are:

$$NO + h\nu \rightarrow N + O \quad J \sim 10^{-5} s^{-1} \qquad (20)$$

$$N + O_2 \rightarrow NO + O \quad k = 5.5 \times 10^{-12} \exp(-3220/T) \qquad (21)$$

$$N + NO \rightarrow N_2 + O \quad k = 8.2 \times 10^{-11} \exp(-410/T) \qquad (22)$$

These processes are unique to the high-altitude region because of (1) the rapid rate of NO photolysis and (2) the presence of atomic nitrogen at significant concentrations (10^5 to 10^7 cm^{-3}). The latter property of these regions is important because it provides a natural sink of NO at these altitudes. Thus, the calculated lifetime of NO in the presence of 10^6 cm^{-3} of N is about one day. Obviously this time is short compared to the time required for the NO to diffuse out of the region to lower altitudes, which is of the order of weeks (see Section II). It follows, therefore, that a high-altitude injection of NO will be much less effective, in terms of final NO_x concentrations achieved, than the corresponding injections directly in the stratosphere. *Since we have already shown that the direct stratospheric injections are not harmful, the input to the stratosphere of injections at higher altitudes is even less effective.*

Another consequence of the presence of NO will be the net local production of odd atomic oxygen, as opposed to the catalytic destruction predominant at lower altitudes. The difference arises from the fact that at high altitudes the O_3 concentration is relatively low (so that $O_3 + NO$ is slow), whereas both J and [N] are high. Thus, the rate of production of atomic oxygen by the reactions written above exceeds the rate of catalytic destruction of odd oxygen by NO_x.

By way of summary, we have concluded that (1) N_2O_4 injected at a high altitude will be largely destroyed before it reaches the stratosphere, and (2) there will be a transitory localized net production of odd oxygen. Because of the temporary and localized nature of the production of atomic oxygen, no practical or harmful consequences are expected to occur.

F. NO_x Ion Chemistry

The terminology used when discussing the upper atmosphere reflects the subject matter. Discussions of neutral chemistry refer to the 50 to 90 km and 90 to 120 km regions of the atmosphere as the mesosphere and thermosphere, reflecting the ambient temperature as the distinguishing characteristic. Overlapping this region is the ionosphere which starts at 60 km and extends upward. This reflects the elevated concentration of ions that first become significant at 60 km.

Our purpose in this section is to summarize briefly the significant properties of the natural ionosphere, and to describe the perturbations to be expected as a result of the propellant release. We will be concerned only with the D-region, which extends from 60 to 90 km, and the E-region, which extends from 90 to 120 km.

In the D-region, ionization results almost exclusively from photoionization of naturally-occurring NO by the Lyman-α line at 1215 Å.

$$NO + h\nu \rightarrow NO^+ + e \qquad (23)$$

($J = 5 \times 10^{-7}$ at zero optical depth)

With an ionization potential of only 9.25 eV, corresponding to 1340 Å, NO is the only atmospheric constituent that can be ionized by this radiation. Shorter wavelengths do not penetrate to these levels. Although NO^+ is the major primary ion formed in the D-region, it is not the dominant ion at all altitudes in this region because other ions are produced by secondary, change transfer reactions leading mainly to hydrated protons, $H(H_2O)_n^+$, and hydrates of NO^+. The NO^+ tends to be more dominant near the top of the D-region, whereas the hydrated ions become relatively more prevalent at lower altitudes (Ref. 35).

Above 90 km, in the E-region, radiation of shorter wavelength is present, and photoionization of O_2 becomes the dominant process (however, photoionization of N_2 is also important):

$$O_2 + h\nu\ (\lambda < 1027\ \text{Å}) \rightarrow O_2^+ + e \qquad (24)$$

Nevertheless, NO^+ continues to be a major ion in the E-region, because it is formed rapidly by such charge exchanges as:

$$O_2^+ + NO \rightarrow NO^+ + O_2 \qquad (25)$$

The steady-state concentration of any given ion, in either region, is determined by the balance between the rates of production and the rates of destruction of that particular ion. Production mechanisms are direct photoionization by sunlight, and charge exchange from other ions. The major loss mechanisms are charge exchange to other species and (for polyatomic ions) dissociative recombination with electrons:

$$O_2^+ + e \rightarrow O + O \qquad (26)$$

Since photoionization of NO is the major source of ion production in the D-layer, the density of charged particles will be increased in that region during the period of time in which the concentration of the dispersing NO cloud is comparable to or greater than the ambient NO concentration, which is in the range of 10^7 to 10^8 cm^{-3}. Based on our plume dispersal calculations, these concentrations will be maintained only for about one day following release.

The increase in the charged particle density can be calculated from the following steady-state equation:

$$\frac{d[E]}{dt} = J(\text{photoion})[NO] - \alpha[NO^+][e] = 0$$

where [e] is the electron concentration, J(photoion) is the rate coefficient for photoionization of NO, and α is the rate coefficient for dissociative recombination of the ion-electron pair. Since $[NO^+] = [e]$, we have

$$[e] = \left(\frac{J[NO]}{\alpha}\right)^{1/2}$$

At zero optical depth, J(photoion) is 5×10^{-7} s^{-1}, decreasing to about 10^{-9} s^{-1} at 60 km (Ref. 36). The quantity α is 8×10^{-7} cm^3/s at 220 K (Ref. 35).

In the E-region, the effect of added NO in increasing the ion density will be somewhat less important, owing to the fact that photoionization of O_2 and N_2, rather than NO, is the major source of ion production in that region. Relative photoionization rates for NO compared to O_2 and N_2 in the E-region show that ambient NO accounts for 1% or less of the total photoionization rate (Ref. 35). Thus, it follows that a significant increase in charge density will occur only when the added NO is about two orders of magnitude greater than the ambient NO, i.e., greater than 10^9 to 10^{10} cm^{-3}. This condition does not prevail for any significant period of time following release.

NO in the E-layer will also have the effect of depleting the densities of other ions such as O_2^+ and N_2^+, since, as already mentioned, these species undergo change-transfer reactions with NO:

$$N_2^+ + NO \rightarrow N_2 + NO^+ \qquad (27)$$

To summarize, addition of NO to the ionospheric region will (1) result in increases in the ion density, and (2) change the relative ionic composition when the concentration of added NO is greater than that of the natural atmosphere. However, as shown in Section II, the latter condition prevails only for a short time, and only on a localized basis. When fully mixed, the added NO concentrations are inconsequentially small compared to the ambient levels. At the present time, the transitory effects occurring on a localized basis are not known to pose any threat to atmospheric stability, nor to produce any effects of a harmful or deleterious nature.

V. Fluorine in the Atmosphere

A. Background

This chapter deals with the atmospheric injection of a propellant that contains fluorine, principally as F_2. The magnitudes of the pertubations to the stratospheric ozone layer and the mesospheric/thermospheric ion content are based on a detailed consideration of fluorine and other neutral and ion chemistries.

Over 1.6×10^5 metric tons (1.7×10^5 tons) of fluorine were used in the manufacture of 6.9×10^5 metric tons (7.6×10^5 tons) of chlorofluoromethanes (CFMs) worldwide in 1973 (Ref. 37). About 81% of this was manufactured for aerosol propellant uses that would bring about a short-term release of the CFMs to the atmosphere. While chlorine from this and other sources has been extensively investigated and modeled for its effect on the chemistry of the stratosphere, fluorine has been largely ignored. Preliminary models of stratospheric fluorine chemistry have been made by Rowland and Molina (Ref. 38) and Stolarski and Rundel (Ref. 39). There are no detailed models that have attempted to describe any perturbations to the ambient concentrations of the mesosphere by the injection of halogen-containing species.

Rowland and Molina point out that F and FO can react with odd oxygen [$O(^3P)$ and O_3] in a manner analogous to chlorine:

$$F + O_3 \rightarrow FO + O_2 \qquad (10)^3$$

$$FO + O \rightarrow F + O_2 \qquad (13)$$

However, they emphasize the differences in rates of reaction and energetics of these two halogens, principally with regard to abstraction reactions of F with CH_4 and H_2 (H atom abstraction from H_2O was neglected.) On this basis they predict that, *relative to Cl, very little odd oxygen will be*

[3] All reaction numbers in this chapter are consistent with Tables 9 and 10.

destroyed before F is converted to HF. They further point out that the HF molecules formed are very strongly bonded (bond dissociation energy = 135 kcal $mole^{-1}$), and therefore are not subject to OH radical attack. Also, HF does not photodissociate at a significant rate in the 1800 to 2200 Å region. Thus, they concluded that, although the stratospheric concentrations of FX and ClX resulting from CFM dissociation will be comparable, the FO_x reaction chain removing O_3 can be disregarded relative to the ClO_x chain.

Stolarski and Rundel (Ref. 39) continued in this area by generating a simple but incomplete model of stratospheric fluorine chemistry based on the following reactions:

$$F + O_3 \rightarrow FO + O_2$$

$$F + H_2 \rightarrow HF + H$$

$$F + CH_4 \rightarrow HF + CH_3$$

$$HF + h\nu \rightarrow H + F$$

$$FO + O \rightarrow F + O_2$$

$$FO + NO \rightarrow F + NO_2$$

$$FO + O_3 \rightarrow F + 2O_2$$

$$HF + O(^1D) \rightarrow OH + F$$

Using available experimental and estimated reaction rate data, they calculated that the catalytic efficiency of fluorine, for ozone destruction, is less than that for chlorine by at least four orders of magnitude. Hence, they concluded that catalytic ozone destruction due to fluorine is negligible relative to that due to chlorine and further that, since hydrogen-bearing compounds are present at parts-per-million levels, HF formation will not cause significant RH compound depletion at stratospheric FX concentrations below parts-per-billion levels.

Recently, several groups of investigators have endeavored to measure present-day fluorine profiles in the stratosphere. Zander, et al., (Ref. 40) measured hydrofluoric acid in the upper stratosphere, and reported a value for the mixing ratio of $\sim 3 \times 10^{-10}$ above 28 km. Based on their ground and balloon-borne observations, they estimate over 50% of the atmospheric HF is above 25 km. Morz, et al., (Ref. 41) utilized balloons and aircraft-borne filter samplers to determine fluoride levels during all four seasons at altitudes of 15 to 40 km. The average of the observed mixing ratio values (v/v) ranged from $\sim 1.5 \times 10^{-11}$ at 17 km, to $\sim 1.1 \times 10^{-10}$ between 25 and 37 km. The data showed considerable variability (a factor of 2) at all altitudes above 17 km. More recently, Farmer and Raper (Ref. 42) used the Jet Propulsion Laboratory High-Speed Interferometer in a balloon-borne gondola to measure HF and the ratio of HF to HCl. In the 14 to 38 km region, they obtained a ratio of 0.1 ±50%. The HF profile as a function of altitude is illustrated in Fig. 18 (Ref. 43).

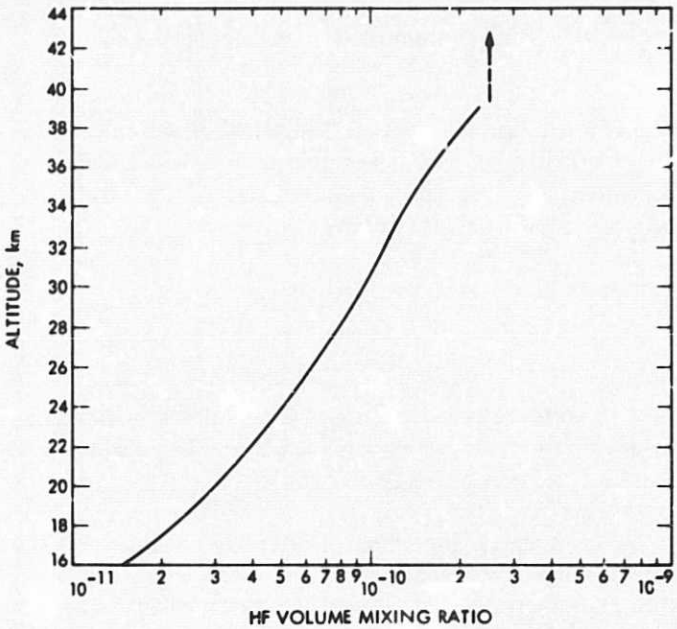

Fig. 18. Profile of the HF Mixing Ratio in the Atmosphere

B. Approach

Atmospheric modeling is immensely complex, involving such factors as horizontal and vertical transport, solar radiation, known and estimated constituent concentrations and fluxes, known and estimated reaction rates, and others. Several such models have been generated for chlorine to predict the impacts of increased atmospheric ClX (ClX = HCl + $ClONO_2$ + ClO + Cl) from CFMs and from the Space Shuttle exhaust effluent. In using such models, an amount of ClX is assumed to be injected, and the resultant change in ozone levels is predicted based on the efficiency with which the ClO_x(Cl + ClO) catalytically destroys odd oxygen.

To assess the effects of the fluorine injection, we have taken advantage of the analogy to chlorine. The first step was to tabulate the heats of formation of relevant species, as listed in Table 9. A comprehensive set of stratospheric reactions that

Table 9. Heats of formation for key species

Species	ΔH_f(298 K)
F	19
F_2	0
HF	-65.3
FO	26
FO_2	3
O	59.6
O_2	0
O_3	34.1
O^1D	104.8
H	52.1
H_2	0
OH	9.3
HO_2	5
H_2O	-57.8
H_2O_2	-32.6
NO	21.6
NO_2	7.9
NO_3	17
NOF	-15.4
HNO_3	-32.3
CH_3	33.2
CH_4	-17.9
CH_3O	3.9
HOF	-23.5
CH_3OO	+6.7

involve fluorine-containing species (FX ≡ HF, F, FO, FO_2, HOF, and NOF) was then assembled (Table 10), from which were chosen those reactions (Table 11) judged to be important. Figure 19 summarizes the resulting fluorine chemistry. These reactions were, in turn, used to formulate two possible chemical models (I and II), whereby the injection of fluorine into the stratosphere would result in the destruction of odd oxygen. A set of analytic expressions was then developed that describes the catalytic efficiency with which FO_x destroys odd oxygen at steady state. Using the chlorine reactions listed in Table 12, an analogous analytic expression was then developed to describe the steady-state catalytic

Table 10. Reactions considered for the fluorine model

Reaction	ΔH, kcal mole^{-1}	Comment or footnote
$*F_2 + h\nu \rightarrow F + F$	38	Dominant initiation process
$F_2 + O \rightarrow F + FO$	-14.6	a
$F_2 + H \rightarrow F + HF$	-98.4	a
$F_2 + NO \rightarrow FNO + F$	-18.0	Possibly an important initiation process
$*F + O_3 \rightarrow FO + O_2$	-27.1	Odd oxygen destruction and FO generation
$*F + O_2 + M \rightarrow FO_2 + M$	-16	Major FO_2 formation mechanism
$*F + H_2 \rightarrow HF + H$	-32.2	b
$*F + H_2O \rightarrow HF + OH$	-17.2	b
$*F + CH_4 \rightarrow HF + CH_3$	-33.2	b
$F + H_2O_2 \rightarrow HF + HO_2$	-109.5	a
$F + HO_2 \rightarrow HF + O_2$	-89.3	a
$F + HNO_3 \rightarrow HF + NO_3$	-35	a
$HF + h\nu \rightarrow F + H$	136.4	Unimportant stratospheric process; low photon flux at relevant wavelengths. Important above 80 km; Lyman-α photolysis
$*HF + O(^1D) \rightarrow F + OH$	-11.2	Dominant stratospheric HF sink; regenerates active fluorine
$HF + OH \rightarrow F + H_2O$	17.2	Unimportant; slow reaction rate
$HF + OH\ (v'' \geq 2) \rightarrow F + H_2O$	–	Exothermic; possibly an important process
$FO + h\nu \rightarrow F + O$	52.6	d; probably unimportant relative to other FO mechanisms
$FO + FO \rightarrow F + F + O_2$	-14	Unimportant at low FO_x concentrations
$*FO + O \rightarrow F + O_2$	-66.6	Loss mechanism for odd oxygen
$FO + O_3 \rightarrow F + O_2 + O_2$	-14.1	c
$FO + O_3 \rightarrow F + O_2 + O_2$	-57.1	c
$*FO + NO \rightarrow F + NO_2$	-20.7	d
$FO + H \rightarrow HF + O$	-83.8	important process in the upper mesosphere
$FO + H_2 \rightarrow HF + OH$	-90.0	d and e
$FO + H_2O \rightarrow HF + HO_2$	-28.5	d and e
$FO + CH_4 \rightarrow HF + CH_3O$	-69.5	d and e
$FO + H_2O_2 \rightarrow HF + OH + O_2$	-49.4	a
$FO + HO_2 \rightarrow HF + O_3$	-62.2	a

Table 10 (contd)

Reaction	ΔH, kcal mole^{-1}	Comment or footnote
$FO + CH_4 \rightarrow HOF + CH_3$	+1.6	d and f
$FO + H_2O \rightarrow HOF + H$	+2.6	d and f
$FO + H_2 \rightarrow HOF + OH$	+17.6	d
$FO + H_2O_2 \rightarrow HOF + HO_2$	-11.9	d
$FO + HO_2 \rightarrow HOF + O_2$	-54.5	d
$FO_2 + h\nu \rightarrow FO + O$	82.6	d; probably unimportant relative to other FO_2 loss mechanisms
*$FO_2 + O \rightarrow FO + O_2$	-36.6	c
*$FO_2 + O_3 \rightarrow FO + O_2 + O_2$	-11.1	c
$FO_2 + H_2 \rightarrow HF + HO_2$	-63.3	g
$FO_2 + H_2O \rightarrow HF + O_2 + OH$	-1.2	g
$FO_2 + CH_4 \rightarrow HF + CH_3OO$	-43.7	g
$FO_2 + H_2O_2 \rightarrow HF + O_2 + HO_2$	-30.7	g
$FO_2 + HO_2 \rightarrow HF + O_2 + O_2$	-73.3	g
$FO_2 + HNO_3 \rightarrow HF + O_2 + NO_3$	-19.0	g
$FO_2 + H_2 \rightarrow HF + H + O_2$	-15.9	g
$FO_2 + CH_4 \rightarrow HF + CH_3 + O_2$	-16.9	g
$FO_2 + NO \rightarrow FO + NO_2$	9.3	d and f
$FO_2 + NO \rightarrow FNO + O_2$	-39.8	g
$FO_2 + H \rightarrow HF + O_2$	-10.2	Important process in the mesophere

*Denotes an important reaction.
[a]Unimportant due to low nonfluorine reactant concentration.
[b]Significant loss mechanism for active fluorine.
[c]Possibly significant mechanism for odd oxygen destruction.
[d]Inhibits odd-oxygen destruction.
[e]Possibly significant loss mechanism for active fluorine; (see Section V).
[f]Although ΔH appears to indicate that the reaction is endothermic and therefore slow, the magnitude of the uncertainties in the heats of formation of FO, FO_2, and HOF are such that the reactions could at least be thermoneutral thus possibly allowing the reactions to proceed at a significant rate.
[g]Will decrease FO_x catalytic efficiency if FO_2 loss mechanism is significant.

efficiency for the ClO_x destruction of odd oxygen. The analytic expressions for FO_x and ClO_x were then compared to estimate the relative efficiencies of the two odd-oxygen scavengers. Thus, making use of explicit perturbation predictions from one-dimensional models for chlorine, the effect of fluorine can be assessed.

Subsections C and D show the steady-state expressions that have been devised to describe the catalytic destruction of odd oxygen by chlorine and fluorine, respectively. These analytic

Table 11. Reactions and numbering system used in stratospheric fluorine model

Reaction	Reaction No.
$F_2 + h\nu \rightarrow F + F$	(9)
$F + O_3 \rightarrow FO + O_2$	(10)
$F + O_2 + M \rightarrow FO_2 + M$	(11)
$F + RH \rightarrow HF + R$	(12)
$FO + O \rightarrow F + O_2$	(13)
$FO + NO \rightarrow F + NO_2$	(14)
$FO + RH \rightarrow HF + RO$	(15)
$FO + O_3 \rightarrow F + 2O_2$	(16)
$FO + O_3 \rightarrow FO_2 + O_2$	(17)
$FO_2 + O_3 \rightarrow FO + 2O_2$	(18)
$FO_2 + O \rightarrow FO + O_2$	(19)
$FO_2 + RH \rightarrow HF + RO_2$	(20)
$HF + O(^1D) \rightarrow F + HO$	(21)
$RH = H_2O, CH_4, H_2$	

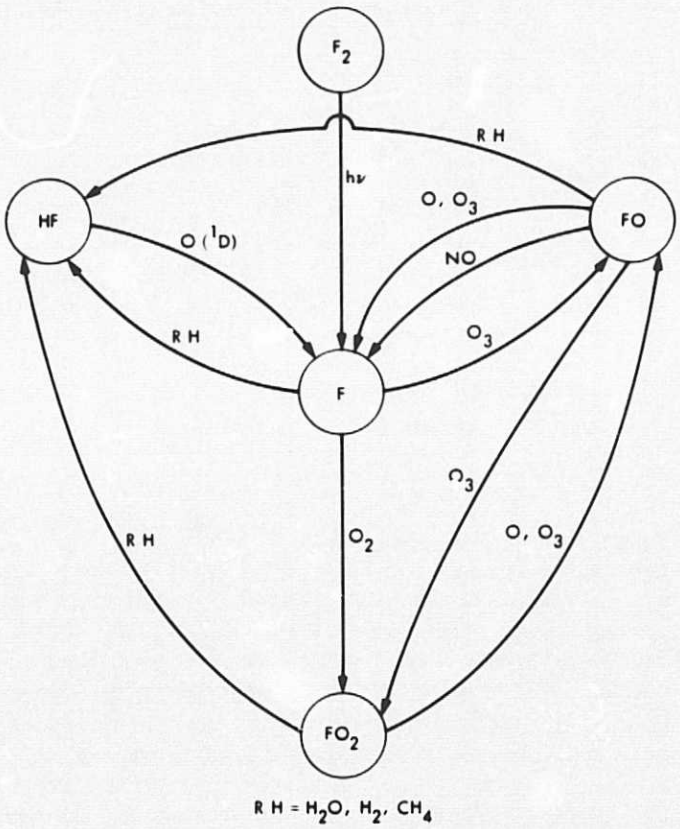

Fig. 19. Schematic diagram of the stratospheric fluorine model

Table 12. Reactions and numbering system used in stratospheric chlorine model

Reaction	Reaction No.
$Cl + O_3 \rightarrow ClO + O_2$	(1)
$ClO + O \rightarrow Cl + O_2$	(2)
$ClO + NO \rightarrow Cl + NO_2$	(3)
$Cl + RH \rightarrow HCl + R$	(4)
$HCl + OH \rightarrow Cl + H_2O$	(5)
$ClO + NO_2 + M \rightarrow ClONO_2 + M$	(6)
$ClONO_2 + h\nu \rightarrow ClO + NO_2$	(7)
$RH = H_2, CH_4, HO_2$	

expressions represent the catalytic efficiency after the systems have attained photochemical steady state. For the case of F_2, photochemical equilibrium is reached after the F_2 has been completely photolyzed (this takes ~16 hours after injection).

The plume chemistry prior to the attainment of steady-state conditions is qualitatively described in Subsection G. We have not developed our own one-dimensional model, where photochemistry is coupled to parameterized transport in the vertical direction, because this type of model is inadequate to describe either the short- or long-term perturbations caused by the injection of a pollutant in a plume. Therefore, we calculate the plume volume (FX concentration) as a function of time (see Section II) and then estimate the steady state ozone perturbation at a series of times after the initial injection of the pollutant utilizing the analytical expressions.

C. The Stratospheric Chlorine Model

Atmospheric chlorine has natural as well as anthropogenic sources. Natural sources include sea spray, volcanoes, and such others as CH_3Cl. Anthropogenic sources include the Space Shuttle main engines and CFMs. Basic kinetic chlorine models incorporate all the reactions and photochemical processes that are considered important in the O_x, HO_x, NO_x, and ClO_x systems.

Although some 10 to 20 reactions involving chlorine-containing species are used in the model calculations, the basic reaction scheme can be described by the reactions listed in Table 12. Using this matrix of reactions, the catalytic destruction of odd oxygen can be described by an analytic expression for the rate of odd-oxygen destruction, $-d(O + O_3)/dt$:

$$\frac{-d(O + O_3)}{dt} = k_1(Cl)(O_3) + k_3(O)(ClO) - k_3(NO)(ClO) \qquad (A)$$

Steady-state expressions for [Cl], [ClO], $[ClONO_2]$ and [HCl] can be derived:

$$[Cl]_{ss} = \frac{k_5(OH)(HCl)}{k_4(RH)} \qquad (I)$$

$$[ClO]_{ss} = \frac{k_1(Cl)(O_3) + J(ClONO_2)}{k_2(O) + k_3(NO) + k_6(NO_2)(M)} \qquad (II)$$

$$[ClONO_2]_{ss} = \frac{k_6(NO_2)(ClO)}{J_7} \qquad (III)$$

$$[HCl]_{ss} = \frac{k_4(Cl)(RH)}{k_5(OH)} \qquad (IV)$$

Substitution of expressions I and II into equation (A) yields an analytic expression that describes the catalytic efficiency of ClO_x in terms of the concentration of the dominant chlorine-containing species, HCl.

$$\frac{-d}{dt}(O_x) = \frac{2k_1k_5(OH)(O_3)(HCl)}{k_4(RH)} \times \frac{k_2(O)}{k_2(O) + k_3(NO)} \qquad (B)$$

Equation (B) is a key result, and will be compared with analogous equations for fluorine to assess the fluorine effect on ozone. The expression, (B), is the same whether or not reactions (6) and (7) are included in the mechanism. The effect of including these two reactions is to reduce [HCl]. However, the theoretical models show that the $[ClONO_2]/[HCl]$ ratio is typically small.

D. The Stratospheric Fluorine Models

Whereas considerable work has been done on stratospheric chlorine chemistry, and there is a consensus as to the principal aspects of the model, stratospheric fluorine chemistry is much less certain. Reaction kinetics are known for very few reactions. In our approach, analytic expressions have been derived for two possible fluorine models that are consistent with the available experimental data. These are then evaluated individually. Two models were used to avoid the complexity that would result if all the possible reactions were incorporated into a single model.

Fluorine may conceptually be partitioned into two states, HF and FO_x (x = 0, 1, 2). HF is very stable and unreactive, whereas FO_x can catalytically destroy odd oxygen and hence ozone.

Our models represent stratospheric fluorine neutral chemistry using the most important reactions and the best reaction rate data available. The point of the models is to determine how much of the fluorine remains as FO_x (destroying odd oxygens) once equilibrium is reached.

Since the factor determining the magnitude of odd-oxygen destruction is the partitioning of F as HF and FO_x, the key factors in generating the models are those reaction rates that affect either the hydrogen abstraction reactions ($FO_x + RH \rightarrow HF + RO_x$) or those reactions that compete with hydrogen abstraction reactions.

1. Fluorine model (I). A distinguishing feature of this model is that the FO_2 radical is formed only via the $F + O_2 + M$ reaction (11), and is not a product of the $FO + O_3$ reaction. It is assumed that the dominant channel in the $FO + O_3$ reaction results in the formation of atomic fluorine and molecular oxygen (16) rather than the FO_2 radical and molecular oxygen (17). Model II differs in this respect, as will be seen. The present reaction system can be written:

$$F_2 + h\nu \rightarrow F + F \quad (9)$$

$$F + O_3 \rightarrow FO + O_2 \quad (10)$$

$$F + O_2 + M \rightarrow FO_2 + M \quad (11)$$

$$F + RH \rightarrow HF + R \quad (12)$$

$$O + FO \rightarrow F + O_2 \quad (13)$$

$$NO + FO \rightarrow NO_2 + F \quad (14)$$

$$RH + FO \rightarrow HF + RO \quad (15)$$

$$O_3 + FO \rightarrow F + 2O_2 \quad (16)$$

$$FO_2 + O_3 \rightarrow FO + 2O_2 \quad (18)$$

$$FO_2 + O \rightarrow FO + O_2 \quad (19)$$

$$FO_2 + RH \rightarrow HF + RO_2 \quad (20)$$

$$HF + O(^1D) \rightarrow F + OH \quad (21)$$

It will be noted that there are three reactions (12, 15, and 20) by which FO_x is converted to the inactive reservoir, HF. The only one of these three reactions definitely known to occur is (12); reactions (15) and (20) have been included for the sake of completeness because they are energetically feasible, although the rates are unknown (see Table 13). In our assessment, several possible values of the rate constant for reaction (15) will be considered to illustrate the effect of this reaction in reducing the catalytic efficiency of fluorine. Reaction (20), which has a similar effect, will not be incorporated explicitly into the analytic expressions, since to do so would introduce needless complexity into the algebraic relationships. This is equivalent to assuming that $k_{20} = 0$, which gives a worst case evaluation of the fluorine impact on ozone. That is, if k_{20} is in fact finite, then fluorine will be even less efficient for ozone destruction.

In our proposed reaction systems, the only mechanism by which the inactive HF is converted to one of the active forms of FO_x is reaction of HF with electronically excited oxygen atoms (O^1D). Photolysis of HF in the stratosphere is an unimportant process, and thus is not considered in our model. However, photolysis becomes significant in the mesosphere and thermosphere (see later discussion). The only additional process that might convert HF to atomic fluorine at a significant rate is:

$$HF + OH(v'' \geq 2) \rightarrow H_2O + F$$

This reaction, and its implications on stratospheric fluorine chemistry, are discussed in Subsection F of this Section.

The net rate of odd oxygen removal for Model I can be written:

$$\frac{-d[O_x]}{dt} = \frac{-d[O + O_3]}{dt} = k_{10}(F)(O_3) + k_{13}(O)(FO) + k_{16}(FO)(O_3)$$

$$- k_{14}(FO)(NO) + k_{18}(FO_2)(O_3) + k_{19}(FO_2)(O)$$

Table 13. Experimental values for fluorine reaction rate constants

Reference	Rate constant/cm^3 $molecule^{-1}s^{-1}$	Temperature, k	Footnote
$H + F_2 \rightarrow HF + H$			
Albright, Dodovov, Lavrovskaya, Morzov and Tal'roze, 1969 (Ref. 44)[a]	$(2.0 \pm 0.16) \times 10^{-10} \exp(-1262 \pm 100/T)$	294 to 565	
Rabideau, Hecht and Lewis, 1972 (Ref. 45)	$(4.2 \pm 0.3) \times 10^{-12}$	300	
Preferred value	$2.4 \times 10^{-10} \exp(-1262/T)$	194 to 565	a
$F_2 + NO \rightarrow NOF + F$			
Rapp and Johnston, 1960 (Ref. 46)	$1.0 \times 10^{-12} \exp(-(757 \pm 50)/T)$	195 to 298	
Kim, Maclean, and Valance, 1972 (Ref. 47)	7.8×10^{-15}	~325	
Preferred value	None		b
$F + O_3 \rightarrow FO + O_2$			
Wagner, Zetzsch and Warnatz, 1972 (Ref. 48)	$2.8 \times 10^{-11} \exp(-226/T)$	253 to 365	
$F + O_2 + M \rightarrow FO_2 + M$			
Zetzsch, 1973 (Ref. 49)	$5.2 \times 10^{-34} \exp(656/T)$, M = He	272 to 362	
Arutyunov, Popov and Chaikin, 1976 (Ref. 50)	$(7 + 2) \times 10^{-33}$ cm^6 $molecule^{-2}s^{-1}$, M = He	293	
	$(1.4 \pm 4) \times 10^{-32}$ cm^6 $molecule^{-2}s^{-1}$, M = N_2	293	
Chen, Trainor, Center and Fyfe, 1977 (Ref. 51)	$(5.4 \pm 0.6) \times 10^{-33}$ cm^6 $molecule^{-2}s^{-1}$, M = He	298	
	$(1.5 \pm 0.3) \times 10^{-32}$ cm^6 $molecule^{-2}s^{-1}$, M = O_2	298	
	$(2.5 \pm 0.5) \times 10^{-30}$ cm^6 $molecule^{-2}s^{-1}$, M = HF	298	
	$(5.0 \pm 0.6) \times 10^{-33}$ cm^6 $molecule^{-2}s^{-1}$, M = F_2	298	
Preferred value	$1.25 \times 10^{-33} \exp(656/T)$, M = N_2	272 to 362	c
$FO + FO \rightarrow 2F + O_2$			
Wagner, Zetzsch and Warnatz, 1972 (Ref. 48)	3.3×10^{-11}	298	
Clyne and Watson, 1974 (Ref. 52)	$(8.5 \pm 2.8) \times 10^{-12}$	298	
Preferred value	1.5×10^{-11}	298	d
$F + H_2 \rightarrow HF + H$			
Homann, Soloman, Warnatz, Wagner and Zetzsch, 1970 (Ref. 53)[a]	$2.63 \times 10^{-10} \exp(-805/T)$ 1.77×10^{-11}	300 to 400 298	
Dodonov, Lavrovskaya, Morozov and Tal'roze, 1971 (Ref. 54)[a]	$(3.0 \pm 1.0) \times 10^{-11}$	293	
Foon and Reid, 1971 (Ref. 55)	$8.05 \times 10^{-11} \exp(-1243/T)$	253 to 348	
Bozzelli, 1972 (Ref. 56)[a]	$(2.5 \pm 0.7) \times 10^{-11}$	~297	
Kompa and Wanner, 1972 (Ref. 57)	6.3×10^{-11}	298	

Table 13 (contd)

Reference	Rate constant/cm^3 molecule^{-1}s^{-1}	Temperature, k	Footnote
Rabideau, Hecht and Lewis, 1972 (Ref. 58)[a]	$(6.6 \pm 1.7) \times 10^{-12}$	293	
Clyne, McKenny and Walker, 1973 (Ref. 59)	$(2.5 \pm 50\%) \times 10^{-11}$	298	
$F + H_2 \rightarrow HF + H$			
Igoshin, Kulakov and Nikitin, 1974 (Ref. 60)	$1.55 \times 10^{-10} \exp(-544/T)$ 2.5×10^{-11}	195 to 296 296	
Lam Thank My, Peron and Puget, 1974 (Ref. 61)	2.3×10^{-12}	300	
Preferred value	2.0×10^{-10}	200 to 400	e
$F + H_2O \rightarrow HF + OH$			
Zetzsch, 1971 (Ref. 62)	$2.0 \times 10^{-11} \exp(-200/T)$	–	
$F + CH_4 \rightarrow HF + CH_3$			
Fettis and Knox, 1964 (Ref. 63)	$2.0 \times 10^{-10} \exp(-609/T)$		
Foan and Reid, 1971 (Ref. 55)	$6.6 \times 10^{-11} \exp(-930/T)$	253 to 368	
Wagner, Warnatz and Zetzsch, 1971 (Ref. 64)	$5.5 \times 10^{-10} \exp(-579/T)$ 7.9×10^{-11}	298 to 450 298	
Kompa and Wanner, 1972 (Ref. 57)	7.1×10^{-11}	298	
Clyne, McKenney and Walker, 1973 (Ref. 59)	6.0×10^{-11}	300	
Pollock and Jones, 1973 (Ref. 65)	$\geq 1 \times 10^{-10}$	298	
Preferred value	7.5×10^{-11}	298	

[a]The two values reported for k(300 K) are in fair agreement. Therefore, the preferred Arrhenius expression reflects the mean of the rate constants at 300 K, and the activation energy reported by Albright, et al. (Ref. 44).

[b]These two values differ by an order of magnitude at 300 K, and would probably be in even worse agreement at stratospheric temperatures. However, this reaction is only important in determining the rate of removal of F_2 (assuming that the rate of this reaction is comparable to J_9), not the catalytic efficiency of FO_x.

[c]The preferred value is based upon three factors: (a) the average of the three determinations of k_{He} (~300 K) 5.7×10^{-33}; (b) the ratio of the third body efficiencies reported by Arutyunov et al. (Ref. 50) k_{N_2}: $k_{He} = 2$; and (c) the assumption that the activation energy is not dependent upon the identity of the third body, $E_a(N_2) = E_a(He)$ = value reported by Zetzsch (Ref. 49).

[d]Although the value of k(FO + FO) reported by Clyne and Watson (Ref. 52) was obtained in a more direct manner than that of Wagner et al. (Ref. 64) and as such is less susceptible to error due to the presence of complicating secondary reactions and thus would normally be preferred. The value to be recommended in this assessment is a weighted average of the two studies.

[e]The value at 300 K seems to be fairly well established as $(2.5 \pm 1.5) \times 10^{-11}$; however, the values reported for E/R are somewhat more scattered (544 to 1243 K). Therefore, it was assumed that $A = 2 \times 10^{-10}$ and then E/R was calculated to yield a value of 2.5×10^{-11} at 300 K.

[f]The preferred value was derived from the data of Wagner et al. (Ref. 64), Kompa and Wanner (Ref. 57), Clyne et al. (Ref. 59), and Pollock and Jones (Ref. 65).

$$= k_{10}(F)(O_3) + (FO)\{k_{13}(O) + k_{16}(O_3) - k_{14}(NO)\} + (FO_2)\{k_{18}(O_3) + k_{19}(O)\} \quad \text{(C)}$$

Using a steady-state analysis, which will be valid at long times (discussed in detail later), the following equalities can be derived:

$$[F]_{ss} = \frac{k_{21}(HF)(O^1D) + (FO)\{k_{13}(O) + k_{14}(NO) + k_{16}(O_3)\}}{k_{10}(O_3) + k_{11}(O_2)(M) + k_{12}(RH)} \quad \text{(V)}$$

$$[FO]_{ss} = \frac{k_{10}(F)(O_3) + k_{18}(FO_2)(O_3) + k_{19}(FO_2)(O)}{k_{13}(O) + k_{14}(NO) + k_{15}(RH) + k_{16}(O_3)} \quad \text{(VI)}$$

$$[FO_2]_{ss} = \frac{k_{11}(O_2)(M)(F)}{k_{18}(O_3) + k_{19}(O)} \quad \text{(VII)}$$

$$[HF]_{ss} = \frac{k_{12}(F)(RH) + k_{15}(FO)(HF)}{k_{21}(O^1D)} \quad \text{(VIII)}$$

Substitution yields:

$$\frac{-d[O + O_3]}{dt} = \frac{k_{21}(O^1D)(HF)\{k_{10}(O_3) + k_{11}(O_2)(M)\}\{2k_{13}(O) + 2k_{16}(O_3) + k_{15}(RH)\}}{k_{15}(RH)\{k_{10}(O_3) + k_{11}(O_2)(M)\} + k_{12}(RH)\{k_{13}(O) + k_{14}(NO) + k_{15}(RH) + k_{16}(O_3)\}} \quad \text{(D)}$$

It is useful to reduce equation D to a simpler form which represents the worst case (maximum possible efficiency) for the destruction of odd oxygen by FO_x.

The Worst case: This occurs if the removal of FO by RH (RH = H_2O, CH_4, H_2, or any other H containing species) is slow, i.e., $k_{15} \cong 0$.

$$\frac{-d[O_x]}{dt} = \frac{2k_{21}(O^1D)(HF)\{k_{10}(O_3) + k_{11}(O_2)(M)\}}{k_{12}(RH)} \times \frac{\{k_{13}(O) + k_{16}(O_3)\}}{\{k_{13}(O) + k_{14}(NO) + k_{16}(O_3)\}} \quad \text{(E)}$$

Important analogies between the chlorine and fluorine systems become apparent upon comparison of equations (B) and (E). Quantitative comparisons are made in Subsection F, to assess the absolute catalytic efficiency of fluorine for the destruction of odd oxygen.

2. **Fluorine model (II).** This model differs from the previous one in that it is assumed that the dominant channel for the FO and O_3 reaction is production of $FO_2 + O_2$ (17) rather than $F + 2O_2$ (16). Again, in the derivation of an analytic expression for $-d(O + O_3)/dt$, we assume for the sake of simplicity that $k_{20}(FO_2 + RH \rightarrow HF + RO_2) = 0$. The reaction scheme can be written:

$$F_2 + h\nu \rightarrow F + F \quad (9)$$

$$F + O_3 \rightarrow FO + O_2 \quad (10)$$

$$F + O_2 + M \rightarrow FO_2 + M \quad (11)$$

$$F + RH \rightarrow HF + R \quad (12)$$

$$O + FO \rightarrow F + O_2 \quad (13)$$

$$NO + FO \rightarrow NO_2 + F \quad (14)$$

$$RH + FO \rightarrow HF + RO \quad (15)$$

$$O_3 + FO \rightarrow FO_2 + O_2 \quad (17)$$

$$FO_2 + O_3 \rightarrow FO + 2O_2 \quad (18)$$

$$FO_2 + O \rightarrow FO + O_2 \quad (19)$$

$$HF + O(^1D) \rightarrow OH + F \quad (21)$$

The equations and steady state concentrations that describe this reaction scheme can be written:

$$\frac{-d(O_x)}{dt} = k_{10}(F)(O_3) + (FO)\left\{k_{13}(O) + k_{17}(O_3) - k_{14}(NO)\right\} + (FO_2)\left\{k_{18}(O_3) + k_{19}(O)\right\} \quad (F)$$

$$[F]_{ss} = \frac{k_{21}(O^1D)(HF) + (FO)\left\{k_{13}(O) + k_{14}(NO)\right\}}{k_{10}(O_3) + k_{11}(O_2)(M) + k_{12}(RH)} \quad (IX)$$

$$[FO]_{ss} = \frac{k_{10}(F)(O_3) + k_{18}(FO_2)(O_3) + k_{19}(FO_2)(O)}{k_{13}(O) + k_{14}(NO) + k_{15}(RH) + k_{17}(O_3)} \quad (X)$$

$$[FO_2]_{ss} = \frac{k_{11}(F)(O_2)(M) + k_{17}(O_3)(FO)}{k_{18}(O_3) + k_{19}(O)} \quad (XI)$$

$$[HF]_{ss} = \frac{k_{12}(F)(RH) + k_{15}(FO)(RH)}{k_{21}(O^1D)} \quad (XII)$$

Therefore, by combining these equations, the following expression for $-d(O_x)/dt$ is obtained:

$$\frac{-d(O_x)}{dt} = \frac{k_{21}(O^1D)(HF)\{k_{10}(O_3)+k_{11}(O_2)(M)\}\{2k_{13}(O)+k_{15}(RH)+2k_{17}(O_3)\}}{k_{15}(RH)\{k_{10}(O_3)+k_{11}(O_2)(M)\}+k_{12}(RH)\{k_{13}(O)+k_{15}(RH)+k_{14}(NO)\}} \quad (G)$$

The worst case occurs when $k_{15} = 0$, which simplifies to:

$$\frac{-d(O_x)}{dt} = \frac{2k_{21}(O^1D)(HF)\{k_{10}(O_3)+k_{11}(O_2)(M)\}}{k_{12}(RH)} \times \frac{\{k_{13}(O)+k_{17}(O_3)\}}{\{k_{13}(O)+k_{14}(NO)\}}$$

This equation is discussed in Subsection F in terms of the absolute catalytic efficiency of FO_x.

3. Summary of worst case equations for the fluorine models. This situation occurs when both $k_{15}(FO + RH)$ and $k_{20}(FO + RH)$ are assumed to be zero. Therefore, $-d(O + O_3)/dt$ can be written:

Model (I):

$$\frac{2k_{21}(O^1D)(HF)\{k_{10}(O_3)+k_{11}(O_2)(M)\}}{k_{12}(RH)} \times \frac{\{k_{13}(O)+k_{16}(O_3)\}}{\{k_{13}(O)+k_{14}(NO)+k_{16}(O_3)\}} \quad (E)$$

Model (II):

$$\frac{2k_{21}(O^1D)(HF)\{k_{10}(O_3)+k_{11}(O_2)(M)\}}{k_{12}(RH)} \times \frac{\{k_{13}(O)+k_{17}(O_3)\}}{\{k_{13}(O)+k_{14}(NO)\}} \quad (I)$$

These expressions are similar, the only difference arising from the relative importance of reactions (16) and (17). Both of these reactions refer to the $FO + O_3$ reaction, but give different products (F and FO_2), respectively.

E. Evaluation of Rate Constants for Key Fluorine and Chlorine Reactions

The rate constants that have been experimentally determined for the key fluorine and chlorine reactions are summarized in Tables 13 and 15 respectively. Table 14 summarizes our estimates for those fluorine reaction rate constants that have not been determined experimentally. These rate constants are needed in Subsection F to evaluate the relative efficiencies of ClO_x and FO_x, which are predicted from the analytic expression derived in Subsections C and D.

Notes accompany each table to explain our selection of the preferred values.

Table 14. Estimates of rate constants for those stratospheric fluorine reactions lacking experimental data

Reaction	Rate constant/cm^3 molecule^{-1}s^{-1}		Footnote
$O + FO \rightarrow F + O_2$	5×10^{-11}		a
$NO + FO \rightarrow F + NO_2$	2×10^{-11}		a
$O_3 + FO \rightarrow F + 2O_2$	2×10^{-11}	(i)	b
	2×10^{-12}	(ii)	
	10^{-13}	(iii)	
	10^{-15}	(iv)	
	0	(v)	
$O_3 + FO \rightarrow FO_2 + O_2$	5×10^{-11}	(i)	b
	2×10^{-12}	(ii)	
	10^{-13}	(iii)	
	10^{-15}	(iv)	
	0	(v)	
$FO + RH \rightarrow HF + RO$	0	(i)	c
	10^{-11}	(ii)	
	10^{-13}	(iii)	
	10^{-15}	(iv)	
$FO_2 + O_3 \rightarrow FO + 2O_2$	5×10^{-11}	(i)	d
	10^{-12}	(ii)	
	10^{-15}	(iii)	
	0	(iv)	
$FO_2 + O \rightarrow FO + O_2$	5×10^{-11}		e
$FO_2 + RH \rightarrow HF + RO_2$	0		f
$HF + O(^1D) \rightarrow OH + F$	1×10^{-10}		g
$HF + h\nu \rightarrow H + F$	$J \sim 10^{-6}$ (>80 km)		h
$F_2 + h\nu \rightarrow F + F$	$J \sim 5 \times 10^{-5}$ (altitude independent)		i
$H + FO \rightarrow HF + O$	5×10^{-11}		j
$H + FO_2 \rightarrow HF + O_2$	5×10^{-11}		k

[a]These estimates are probably accurate (2σ) to within a factor of 3 and are based upon the assumption that the reactivity of FO with O(^{3}P) and NO is similar to the reactivity of both ClO and BrO with O(^{3}P) and NO (provisional experimental data supports this assumption). The analogous experimentally determined rate constants for ClO and BrO are: k_2(O + ClO) = 5.0×10^{-11}, k_3(NO + ClO) = 1.85×10^{-11}; k(O + BrO) = (3 ± factor of 3) $\times 10^{-11}$, and k(NO + BrO) = 2.1×10^{-11}. These rate constants are expressed in units of cm^3 molecule^{-1}s^{-1} and were measured at ~300 K. The temperature dependence of the rate constants for these radical-radical processes is expected to be small.

[b]The FO + O_3 reaction has two possible pathways which are exothermic, resulting in the production of F + $2O_2$ (16) or FO_2 + O_2 (17). Although this reaction has not been studied in a simple direct manner, two studies of complex chemical systems have inferred some kinetic information about it. Starrico et al., (Ref. 66) measured quantum yields for ozone destruction in F_2/O_3 mixtures, and attributed the high values, ~4600, to be due to the rapid regeneration of atomic fluorine via the FO + $O_3 \rightarrow$ F + $2O_2$ reaction (16). However, their results are probably also consistent with the chain propagation process being FO + FO $\rightarrow$ 2F + O_2 (the latter reaction has been studied twice by Wagner, et al., 1972; Clyne and Watson, (1974), but although the value of $[F]_{produced}/[F]_{consumed}$ is known to be close to unity, it has not been accurately determined). Consequently it is impossible to ascertain from the experimental results of Starrico et al., whether or not the high quantum yields for ozone destruction should be attributed to the FO + O_3 reaction producing either F + $2O_2$ or FO_2 + O_2 (this process is also a chain propagation step if the resulting FO_2 radical preferentially reacts with ozone rather than with either FO or itself.). Wagner et al., 1972, utilized a low-pressure discharge flow-mass spectrometric system to study the F + O_3 and FO + FO reactions by directly monitoring the time history of the concentrations of F, FO, and O_3. They concluded that the FO + O_3 reaction was unimportant in their system. However, their paper does not present enough information to warrant this conclusion. Indeed, their value of k(FO + FO) of 3×10^{-11} is about a factor of four greater than that reported by Clyne and Watson, 1974, which may possibly be attributed to either reactive impurities being present in their system, e.g., O(3P), or that the FO + O_3 reactions (16, 17) were not of negligible importance in their study. Consequently, it is not possible to determine a value of either k_{16} or k_{17} from existing experimental data. Therefore, in our assessment of the catalytic efficiency of FO_x, a range of values for k_{16} and k_{17} will be assumed (i through v). It is worth noting that the analogous ClO + O_3 reactions are extremely slow (~10^{-18} cm^3 molecule^{-1}s^{-1}), and only an upper limit of 9×10^{-14} has been set for k(BrO + O_3).

[c]There are no experimental data for these reactions. Thus, it is difficult to estimate the likely magnitude of these reaction rate constants. Some analogous ClO reactions have been studied and found to be very slow, e.g., ClO + $H_2 \leq 8 \times 10^{-16}$ (670 K), ClO + $CH_4 \leq 4 \times 10^{-15}$ (670 K). These values would correspond to upper limits of ~10^{-21} and 10^{-19} respectively at 230 K (stratospheric conditions). The fluorine reactions may be somewhat faster due to their greater exothermicity (due to the HF bond being stronger than the HCl bond). Therefore in this assessment we have adopted a range of values for the FO + RH rate constants to test the sensitivity to these reactions. The case considered to be most important is that when k_{15} is assumed to be zero.

[d]No experimental data. A reaction that has been studied that can be considered somewhat comparable is HO_2 + O_3. The literature values for this reaction are in rather poor agreement (especially the values of E/R), but do agree that it is slow at 300 K with a value of ~1.5×10^{-15}. A range of values can be used in the assessment. In the worst case (where k_{20} = 0), it is irrelevant what value of k_{18} is used because the only reaction considered (FO_2 + O_3, and FO_2 + O) both yield the FO radical as a product. Only when k_{20} is given a finite value does the magnitude of k_{18} become important.

[e]The rate constant for such a radical-atom process is expected to approach the gas collision frequency. As for k_{18}, the magnitude of k_{19} is only important for nonzero values of k_{20}.

[f]No experimental data for these or any analogous reactions.

[g]Assumed to be comparable to most other O^{1}D reaction rate constants that approach the gas kinetic collision frequency.

[h] This J value has been derived based on a estimated value for σ(HF) at 121.6 nm (extrapolated from the absorption spectra of HCl, HBr and HI), and the flux of Lyman-α radiation. This is the dominant photochemical loss mechanism for HF in the upper mesosphere (>80 km).

[i] This J value is based on the absorption cross-sections reported for F_2 (Ref. 67), and the calculated J value of $2 \times 10^{-3} s^{-1}$ for Cl_2. This J value is almost independent of altitude, as a major portion of the absorption spectrum is at wavelengths greater than 300 nm.

[j] These rate constants are expected to approach the gas collision frequency. Important loss processes for active FO_x in the mesosphere.

Table 15. Rate constants for reactions in stratospheric chlorine model

Reaction	Rate constant/cm^3 molecule^{-1}s^{-1}
$Cl_2 + h\nu \rightarrow Cl + Cl$	$J \sim 1 \times 10^{-3}$ s^{-1}
$Cl + O_3 \rightarrow ClO + O_2$	$2.7 \times 10^{-11} \exp(-257/T)$
$ClO + O \rightarrow Cl + O_2$	$7.7 \times 10^{-11} \exp(-130/T)$
$ClO + NO \rightarrow Cl + NO_2$	$1.0 \times 10^{-11} \exp(+(200 \pm 100)/T)$
$Cl + CH_4 \rightarrow HCl + CH_3$	$7.3 \times 10^{-12} \exp(-1260/T)$
$Cl + HO_2 \rightarrow HCl + O_2$	3×10^{-11}
$HCl + OH \rightarrow Cl + H_2O$	$3.0 \times 10^{-12} \exp(-425/T)$
$ClO + NO_2 + M \rightarrow ClONO_2 + M$, $M = N_2$	$\frac{3.3 \times 10^{-23} T^{-3.34}}{1 + 8.7 \times 10^{-9} T^{-0.6} M^{0.5}}$
$ClONO_2 + h\nu \rightarrow ClO + NO_2$	$J \sim 3 \times 10^{-5}$ s^{-1} (20 km)
	$\sim 4.6 \times 10^{-5}$ s^{-1} (30 km)
	$\sim 1.9 \times 10^{-4}$ s^{-1} (40 km)
	$\sim 4.2 \times 10^{-4}$ s^{-1} (50 km)
$NO_2 + h\nu \rightarrow NO + O$	$J \sim 5 \times 10^{-3}$ s^{-1}

F. Assessment of Fluorine Catalytic Efficiency

Table 16 shows some typical values of the concentrations of atmospheric species that are predicted by the one-dimensional photochemical models, as a function of altitude. The values of these concentrations were combined with the preferred rate constants shown in Tables 13 to 15 to numerically evaluate values of $-d(O + O_3)/dt$ for both the fluorine (models I and II) and chlorine systems. The calculated values of $-d(O + O_3)/dt$, which are shown in Table 17, represent the worst case situation where both k_{15} and k_{20} are assumed to be zero. The different values shown for $-d(O + O_3)/dt$, (i) through (v), correspond to a range of values for k_{16} (model I) and k_{17} (model II) as indicated in Table 14. Table 18 and Fig. 20 show the ratio of the efficiencies of the fluorine and chlorine systems, $\rho(FO_x)/\rho(ClO_x) = -d(O_x)/dt$ (fluorine)/$-d(O_x)/dt$ (chlorine) on a per molecule basis.

From Tables 17 and 18 it can be seen that the values of $-d(O_x)/dt$ calculated for model II are significantly greater than those for model I. The difference in catalytic efficiencies arises because in model I, F atoms are continually being recycled by reaction 16 ($FO + O_3 \rightarrow F + 2O_2$), and are thus subject to being rapidly converted to HF via reaction 12. In model II, this is not the case, because F atoms are not involved in the cycle that destroys odd oxygen:

$$FO + O_3 \rightarrow FO_2 + O_2 \quad (17)$$

$$FO_2 + O_3 \rightarrow FO + 2O_2 \quad (18)$$

$$FO_2 + O \rightarrow FO + O_2 \quad (19)$$

$$\text{net: } FO_2 + O\,(O_3) \rightarrow FO + O_2\,(2O_2)$$

In both models (especially II) the catalytic efficiency is greatest for high values of $k(FO + O_3)$. Table 19 shows how the catalytic efficiency of FO_x decreases (especially with model II) when the rate constant for the FO + RH reaction (15) is assumed to be nonzero. This reaction (15) provides an additional route by which active FO_x is converted to HF. A nonzero value for the rate constant of the FO_2 + RH reaction (20) would have a similar effect to that of reaction (15).

Tables 17 and 18 show that even in the worst case, the catalytic efficiency of ClO_x normally exceeds that of FO_x. This difference can be attributed to the greater reactivity of atomic F, compared to atomic Cl, towards RH, and the inert nature of HF compared to HCl. The only significant loss mechanism for HF is reaction with electronically excited O^1D atoms, whereas HCl is readily attacked by OH radicals, producing atomic chlorine. The inert nature of HF, and the reactive nature of atomic F manifests itself in a larger percentage of FX being tied up in the form of HF compared to the percentage of ClX in the form of HCl.

As it is impossible to estimate the most probable values for the rate constants of the $FO + O_3$ (16, 17), FO + RH (15) and FO_2 + RH (20) reactions we shall assess the worst case, knowing that in all probability the true catalytic efficiency of FO_x (especially in model II) is at least a factor of 20 to 400 lower.

Table 20 summarizes the mixing ratios of FX that would result from a 50-s dump initiated at 43 km (this is referred to as case (a) in Section II). At times shorter than 10 days, the concentration of FX caused by propellant dumping is greater than ambient (see Fig. 3) where a mixing ratio of ~2.5 X

Table 16. Predicted concentrations of atmospheric species using a one-dimensional model

Species	Altitude, km					
	20	25	30	35	40	45
M	1.95×10^{18}	8.4×10^{17}	3.76×10^{17}	1.72×10^{17}	8.2×10^{16}	4.1×10^{16}
O_2	3.9×10^{17}	1.7×10^{17}	7.5×10^{16}	3.4×10^{16}	1.6×10^{16}	8.2×10^{15}
O^1D	5.6×10^{-1}	3.0	1.2×10	3.8×10	8.4×10	1.2×10^{2}
O^3P	2.0×10^{6}	1.4×10^{7}	6.2×10^{7}	2.4×10^{8}	8.0×10^{8}	2.2×10^{9}
H_2O	6.8×10^{12}	3.2×10^{12}	1.5×10^{12}	7.2×10^{11}	3.9×10^{11}	2.1×10^{11}
CH_4	2.3×10^{12}	9.0×10^{11}	3.0×10^{11}	1.1×10^{11}	4.5×10^{10}	1.5×10^{10}
H_2	1.3×10^{12}	6.3×10^{11}	2.8×10^{11}	1.2×10^{11}	4.9×10^{10}	2.0×10^{10}
HO_2	4.9×10^{7}	6.8×10^{7}	8.5×10^{7}	7.8×10^{7}	5.0×10^{7}	3.4×10^{7}
NO	5.8×10^{8}	7.3×10^{8}	9.8×10^{8}	9.7×10^{8}	9.5×10^{8}	6.7×10^{8}
NO_2	1.9×10^{9}	3.3×10^{9}	3.6×10^{9}	1.8×10^{9}	4.8×10^{8}	6.0×10^{7}
OH	1.1×10^{6}	1.7×10^{6}	3.0×10^{6}	6.3×10^{6}	1.4×10^{7}	1.6×10^{7}
O_3	4.2×10^{12}	5.2×10^{12}	3.8×10^{12}	1.8×10^{12}	5.4×10^{11}	1.4×10^{11}
Temp	218	223	229	234	248	264

10^{-10} (v/v) has been observed at 40 km. Recently (January 1977), a NASA chlorofluoromethane assessment workshop was held to evaluate the stratospheric ozone perturbation caused by the CFMs. Nine research groups calculated the steady-state ozone perturbation that would result from the continued release of CFMs at the 1975 rate using one-dimensional photochemical models. The steady-state concentrations of ClX produced from CFM photodissociation was ~5 ppb and the range of ΔO_3 that was predicted from the models was 5 to 9%. This assessment assumed that the fluorine released from the CFMs did not perturb the ozone concentration. Since this workshop, there has been a redetermination of the $NO + HO_2 \rightarrow NO_2 + OH$ rate constant that results in a doubling of the predicted catalytic efficiency of ClO_x, i.e., 5 ppb ClX reduces the integrated ozone column by 10 to 18%. For this assessment we shall assume that the percentage reduction in ozone is linearly proportional to the ClX mixing ratio (this is not strictly true) and that 5 ppb of ClX causes an 18% reduction in the integrated ozone column. Figure 21 shows the results of the NASA CFM perturbation calculation, and illustrates how the ozone concentration is significantly reduced at 40 km, but is increased between 20 to 25 km predominantly due to the "self-healing" effect (because of the loss of ozone between 30 to 50 km, more ultraviolet radiation penetrates to the lower stratosphere, resulting in more low-altitude production of ozone). The fluorine situation is a little different from that of chlorine for several reasons: (a) at times less than a year, the fluorine resulting from a propellant dump is largely confined to the atmospheric layer in which it was initially deposited, whereas the chlorine resulting from CFM photodissociation is almost uniformly distributed vertically (constant mixing ratio). For the sake of simplicity, we have assumed that the fluorine is well-mixed vertically. This will tend to overestimate the actual ozone loss by a small factor ~(2 to 4); (b) It can be seen from Table 17 that the magnitude of $-d(O_x)/dt$ in the chlorine model monotonically increases with altitude, whereas in fluorine model II the converse occurs. Consequently, it is difficult to obtain an accurate value for the catalytic efficiency of FO_x relative to ClO_x when their relative efficiencies vary with altitude. In this assessment, the relative efficiency of FO_x compared to ClO_x is that predicted in Table 18 at the mean altitude of the released cloud. Table 18 (model II) shows that $\rho(FO_x)/\rho(ClO_x) \leqslant 2.1(-3)$ at 40 km. After one day, when the plume diameter is ~100 km, the ozone perturbation *within the cloud* will be $\rho(FO_x)/\rho(ClO_x) \times \mu(FO_x)/\mu(ClO_x) \times 60\% = 2.1 \times 10^{-3} \times 2.1(-8)/5(-9) \times 60\% = 0.5\%$. The value of 60% for ozone reduction at 40 km is taken from Fig. 21. However, the integrated ozone column will have been reduced by only $<<0.15\%$ (due to the self-healing effect at lower altitudes, and because most of the ozone layer is between 20 and 30 km and the FO_x cloud does not penetrate this region). Consequently, it can be seen that even the short-term localized perturbation is small. After one month, the FO_x concentration due to the propellant dump is only ~5% of the background level, and the ozone perturbation is predicted (worst case) to be $<10^{-4}\%$. After five years the propellant is expected to be well-mixed, both horizontally and vertically, resulting in a mixing ratio of $\sim 10^{-14}$ (more than 4 orders of magnitude less than present-day ambient). Propellant dumps initiated at slightly lower

Table 17. Calculated values for the change in odd oxygen concentrations after a stratospheric fluorine injection[a]

Altitude, km		Model I	Model II	ClO_x model
25	i[b]	$2.4 \times 10^{-8} \times$ [HF]	$4.2 \times 10^{-4} \times$ [HF]	$9.2 \times 10^{-5} \times$ [HCl]
	ii	2.4×10^{-8}	1.6×10^{-5}	
	iii	2.3×10^{-8}	7.9×10^{-7}	
	iv	7.2×10^{-9}	9.2×10^{-9}	
	v	1.2×10^{-9}	1.2×10^{-9}	
30	i	4.5×10^{-8}	3.6×10^{-4}	8.4×10^{-4}
	ii	4.5×10^{-8}	1.5×10^{-5}	
	iii	4.3×10^{-8}	6.6×10^{-7}	
	iv	1.4×10^{-8}	1.4×10^{-8}	
	v	6.0×10^{-9}	6.0×10^{-9}	
35	i	7.1×10^{-8}	2.0×10^{-4}	5.2×10^{-3}
	ii	7.1×10^{-8}	8.0×10^{-6}	
	iii	6.3×10^{-8}	3.9×10^{-7}	
	iv	2.9×10^{-8}	2.9×10^{-8}	
	v	2.7×10^{-8}	2.7×10^{-8}	
40	i	6.7×10^{-8}	3.0×10^{-5}	1.4×10^{-2}
	ii	6.7×10^{-8}	1.3×10^{-6}	
	iii	5.7×10^{-8}	1.0×10^{-7}	
	iv	4.6×10^{-8}	4.6×10^{-8}	
	v	4.6×10^{-8}	4.6×10^{-8}	
45	i	4.7×10^{-8}	2.7×10^{-6}	2.5×10^{-2}
	ii	4.3×10^{-8}	1.5×10^{-7}	
	iii	4.3×10^{-8}	4.7×10^{-8}	
	iv	4.3×10^{-8}	4.3×10^{-8}	
	v	4.3×10^{-8}	4.3×10^{-8}	

[a]Calculated values for $-d(O + O_3)/dt$: worst cases ($k_{15} = k_{20} = 0$)
[b]These lower-case roman numerals correspond to the (i) - (v) range of values estimated for the $FO + O_3$ rate constant shown in Table 14.

Table 18. The ratio of catalytic efficiencies of the fluorine and chlorine systems

Altitude, km		Model I $\rho(FO_x)/\rho(ClO_x)$	Model II $\rho(FO_x)/\rho(ClO_x)$
25	i[a]	2.6×10^{-4}	4.6
	ii	2.6×10^{-4}	0.17
	iii	2.5×10^{-4}	8.6×10^{-3}
	iv	7.8×10^{-5}	1.0×10^{-4}
	v	1.3×10^{-5}	1.3×10^{-5}
30	i	5.4×10^{-5}	0.43
	ii	5.4×10^{-5}	1.8×10^{-2}
	iii	5.1×10^{-5}	7.9×10^{-4}
	iv	1.7×10^{-5}	1.7×10^{-5}
	v	7.1×10^{-6}	7.1×10^{-6}
35	i	1.4×10^{-5}	3.8×10^{-2}
	ii	1.4×10^{-5}	1.5×10^{-3}
	iii	1.2×10^{-5}	7.5×10^{-5}
	iv	5.6×10^{-6}	5.6×10^{-6}
	v	5.2×10^{-6}	5.2×10^{-6}
40	i	4.8×10^{-6}	2.1×10^{-3}
	ii	4.8×10^{-6}	9.3×10^{-5}
	iii	4.1×10^{-6}	7.1×10^{-6}
	iv	3.3×10^{-6}	3.3×10^{-6}
	v	3.3×10^{-6}	3.3×10^{-6}
45	i	1.9×10^{-6}	1.1×10^{-4}
	ii	1.7×10^{-6}	6.0×10^{-6}
	iii	1.7×10^{-6}	1.9×10^{-6}
	iv	1.7×10^{-6}	1.7×10^{-6}
	v	1.7×10^{-6}	1.7×10^{-6}

[a]These lower-case roman numerals correspond to the (i) - (v) range of values estimated for the $FO + O_3$ rate constant shown in Table 14.

altitudes may cause slightly greater ozone reductions because $\rho(FO_x)/\rho(ClO_x)$ is a factor of 200 greater at 30 km than at 40 km. However, even if the catalytic efficiency of FO_x were equal to that of ClO_x, the concentration of FO_x resulting from a propellant dump would be so low that no significant ozone depletion would result after the plume had even partially dispersed.

It is conceivable that, besides conversion of HF to active FO_x via reaction with O^1D, an additional process could be:

$$HF + OH(v'' \geq 2) \rightarrow H_2O + F$$

However, the maximum likely rate constant for the above process is $\sim 10^{-12}$ and at that rate, combined with the predicted values for [OH, $v'' \geq 2$] reported by Nagy et al. (Ref. 68) of $\sim 10^4$ cm^{-3}, the overall catalytic efficiency of FO_x would only increase by less than a factor of ten. Consequently, the catalytic efficiency of FO_x would still be too low to be of importance in terms of releasing small quantities of F_2 from the Space Shuttle.

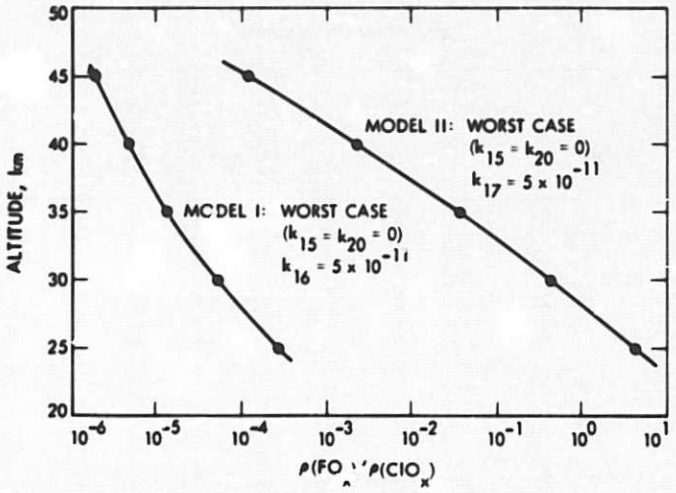

Fig. 20. Ratio of the catalytic efficiencies of stratospheric fluorine and chlorine.

G. Plume Chemistry

Although the equilibrium eventually reached will resemble situations previously discussed, the propellant ejected from the Space Shuttle will initially exhibit "plume" chemistry, involving localized and severe short-term perturbations of the ambient concentrations of the trace constituents. In the immediate vicinity of the Space Shuttle, a transient condition of a very-high concentration of F_2 will exist. The time taken to reach steady-state conditions is governed by the rate of loss of molecular fluorine. The dominant loss mechanism for molecular fluorine is photolysis, with a J value of $\sim 5 \times 10^{-5} s^{-1}$, with reaction with NO being a second minor loss process:

$$F_2 + h\nu \rightarrow F + F$$

$$F_2 + NO \rightarrow F + FNO$$

$$FNO + h\nu \rightarrow F + NO$$

Consequently, the time taken for 95% of the molecular fluorine to be dissociated is about 16 h, assuming that photolysis is the only removal mechanism. It is difficult to ascertain the importance of the NO + F_2 reaction, as the rate constant is uncertain by at least one order of magnitude (Table 13), and, in addition, the NO in the plume may be significantly depleted if FNO photolysis is slow. However, if the NO + F_2 is rapid enough to be competitive with photolysis, its only importance is that the molecular fluorine is removed more rapidly and FO_x attains steady-state conditions earlier. Atomic fluorine formed from the processes shown above reacts with oxygen-containing species (O_3, O_2, and O) to destroy odd oxygen, and hydrogen-containing compounds (RH ≡ H_2O, CH_4, H_2) to produce HF and localized high concentrations of odd-hydrogen radicals such as OH, CH_3, and H. These localized concentrations of odd-hydrogen radicals may far exceed the ambient levels (by many orders of magnitude), and the plume will exhibit a chemistry dominated by radical-radical recombination processes.

While the plume is still highly localized (~half a day) the concentration of RH(H_2O, CH_4, and H_2) will be almost totally depleted by the F + RH reaction, resulting in an effective increased catalytic efficiency for FO_x. The ozone level in the plume will also be significantly, if not totally, depleted However, it is not worth carefully modelling this localized situation as the condition is transitory, and the atmosphere rapidly recovers as the plume disperses. The injection of fluorine is in a region of the stratosphere where the chemical composition is controlled by photochemistry; consequently,

Table 19. Changes in FO_x catalytic efficiency as a function of nonzero rate constants for reaction (15) (FO + RH → HF + RO)

Altitude, km	k_{15}	$k_{16,17} = 5 \times 10^{-11}$		$k_{16,17} = 2 \times 10^{-12}$	
		Model I	Model II	Model I	Model II
30	0	5.4×10^{-5}	0.43	5.4×10^{-5}	1.8×10^{-2}
	10^{-13}	5.4×10^{-5}	2.1×10^{-2}	5.1×10^{-5}	8.1×10^{-3}
	10^{-11}	4.5×10^{-5}	2.3×10^{-4}	1.8×10^{-5}	2.1×10^{-5}
40	0	4.8×10^{-6}	2.1×10^{-3}	4.8×10^{-6}	9.3×10^{-5}
	10^{-13}	4.8×10^{-6}	8.6×10^{-4}	4.4×10^{-6}	3.8×10^{-5}
	10^{-11}	3.8×10^{-6}	1.6×10^{-5}	1.7×10^{-6}	1.9×10^{-6}

Table 20. Mixing ratios of FX following a 50-s duration ejection between 43 km and 36 km[a]

Time	[FX]	FX (v/v)	% F_2 (dissociated)
1 h	5.0×10^{12}	6.3×10^{-5}	17
5.6 h	7.1×10^{10}	8.9×10^{-7}	64
1 day	1.7×10^{9}	2.1×10^{-8}	99
10 day	9.8×10^{6}	1.2×10^{-10}	100
1 mo	1.2×10^{6}	1.4×10^{-11}	100
1 yr	4.7×10^{4}	5.9×10^{-13}	100

[a]Case (a) 50-s dump initiated at 43 km.

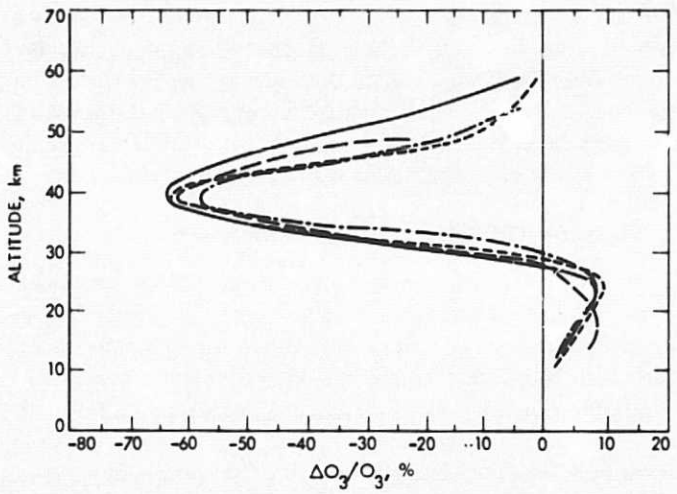

Fig. 21. Perturbation in the ozone concentration resulting from CFMs in the atmosphere.

there will be a rapid regeneration of photochemically produced species such as O_3.

H. Neutral Fluorine Chemistry in the Mesosphere

Neutral fluorine chemistry in the mesosphere is similar to that previously described for the stratosphere. The major differences are that HF will undergo photolytic decomposition by short wavelength UV light (Lyman-α at 121.6 nm) at a rate much greater than its reaction with electronically excited oxygen atoms (O^1D), and that the concentrations of atomic hydrogen, nitrogen, and oxygen are much greater in the mesosphere than in the stratosphere. Consequently, this affects the relative importance of some of the reactions. The chemical scheme can be written:

$$F_2 + h\nu \rightarrow F + F \quad (9)$$

$$F_2 + H \rightarrow HF + F \quad (22)$$

$$F + O_3 \rightarrow FO + O_2 \quad (10)$$

$$F + O_2 + M \rightarrow FO_2 + M \quad (11)$$

$$F + RH \rightarrow HF + R \quad (12)$$

$$O + FO \rightarrow F + O_2 \quad (13)$$

$$NO + FO \rightarrow NO_2 + F \quad (14)$$

$$RH + FO \rightarrow HF + RO \quad (15)$$

$$FO + O_3 \rightarrow F + O_2 + O_2 \quad (16)$$

$$FO + O_3 \rightarrow FO_2 + O_2 \quad (17)$$

$$H + FO \rightarrow HF + O \quad (24)$$

$$FO_2 + O_3 \rightarrow FO + 2O_2 \quad (18)$$

$$FO_2 + O \rightarrow FO + O_2 \quad (19)$$

$$FO_2 + RH \rightarrow HF + RO_2 \quad (20)$$

$$HF + O^1D \rightarrow OH + F \quad (21)$$

$$HF + h\nu \rightarrow H + F \quad (23)$$

The Table 21 shows some typical values expected for concentrations of neutral constituents in the mesosphere (Ref. 69).

A careful analysis of the fluorine reaction scheme listed above shows that about five of these reactions dominate and are sufficient to describe neutral fluorine chemistry. Photolysis remains the major loss process for F_2 until 100 km, when reaction with atomic H becomes comparable. Therefore, the half life of F_2 in the mesosphere is comparable to that in the

Table 21. Concentrations of neutral constituents in molecules/cm³

Species	Altitude, km		
	60	80	100
[M]	7.2×10^{15}	4.2×10^{14}	1.1×10^{13}
[O_2]	1.4×10^{15}	1.1×10^{14}	2.2×10^{12}
[O^1D]	$\sim 3 \times 10^{2}$	$\sim 1 \times 10^{2}$	1.2×10^{3}
[O^3P]	7×10^{9}	6×10^{9}	4×10^{11}
[O_3]	3×10^{9}	1×10^{8}	1×10^{7}
[CH_4]	3.2×10^{8}	6.3×10^{6}	–
[H_2]	3.6×10^{9}	1.7×10^{9}	1.1×10^{7}
[H_2O]	3.5×10^{10}	5.9×10^{8}	7.7×10^{5}
[H]	1.4×10^{6}	3×10^{7}	1.1×10^{8}
[OH]	3×10^{6}	1×10^{6}	--
[HO_2]	3×10^{6}	1×10^{6}	–
[NO]	5×10^{7}	5×10^{7}	5×10^{7}
T,K	253	177	210

stratosphere, ~5.6 h. Due to the decrease in total gas density with altitude, the $F + O_3$ reaction dominates the $F + O_2 + M$ reaction so that primary formation of FO_2 is not particularly important in the mesosphere. The fate of the FO radicals formed in reaction (10) will be dominated by reaction with O^3P, so that reactions (14), (15), (16), and (17) can be neglected. Reaction (24) is of little significance due to the high $[O^3P]/[H]$ ratio. Reactions (18) and (19) can be neglected because the rate of formation of FO_2 via reactions (11) and (17) is unimportant. Therefore, the reaction scheme can be reduced to:

$$F_2 + h\nu \rightarrow F + F \qquad (9)$$

$$F + O_3 \rightarrow FO + O_2 \qquad (10)$$

$$F + RH \rightarrow HF + R \qquad (11)$$

$$FO + O \rightarrow F + O_2 \qquad (13)$$

$$HF + h\nu \rightarrow F + H \qquad (22)$$

The following equations can be derived for $[F]_{ss}$, $[FO]_{ss}$, and $[HF]_{ss}$.

$$[F]_{ss} = \frac{k_{13}(O)(FO) + J_{22}(HF)}{k_1(O_3) + k_{11}(RH)}$$

$$[FO]_{ss} = \frac{k_{10}(F)(O_3)}{k_{13}(O)}$$

$$[HF]_{ss} = \frac{k_{11}(F)(RH)}{J_{22}}$$

Substituting values for the rate constants and concentrations in the above equations shows that HF:F:FO at 80 km is $1:10^{-4}:10^{-6}$; i.e., HF is the dominant fluorine species, as was the case in the stratosphere. The quantity of F_2 ejected into the mesosphere is too low to significantly perturb the concentrations of any of the neutral species after a day or so. For a few hours, the concentrations of RH and O_3 may be depleted in the plume, but, as the plume disperses, the atmosphere rapidly recovers. Consequently, we conclude that the only fate of F_2 injected into the mesosphere is downward transport into the stratosphere in the form of HF, with no adverse effect on the neutral contituents of the mesosphere.

I. Fluorine Chemistry in the Ionosphere

In Section II, it was shown that release of N_2O_4 propellant in the ionosphere would result in temporary, localized changes in charge density and ionic composition, owing mainly to the fact that NO (which is the major product) has a very low ionization potential. For F_2 release, however, no such effects are expected to occur because of the much higher ionization potentials involved. The relevant fluorine species, along with the corresponding ionization potentials, are:

Species	Ionization potential, eV
F_2	15.7
F	17.4
HF	15.8
FO	13 to 14 (uncertain)
FO_2	12.6

Thus, there will be no photoionization of the fluorine species in the D-layer, because radiation of sufficiently short wavelength is not present. In the E region, these species will probably be photoionized with *J*-values similar to those of N_2, since the ionization potentials are similar. However, since the

fluorine concentrations will be small, the resulting effects on the charge density or ion composition will be quite negligible. Furthermore, the principal form in which the fluorine will be present, HF, cannot be ionized by charge exchange from any of the abundant ions in the D- or E-regions (O_2^+, N_2^+, or NO^+), because the ionization energy of HF is greater than that of any of those ions.

We conclude, therefore, that release of F_2 in the ionosphere will not significantly perturb that region.

VI. Summary and Conclusions

If a Space Shuttle flight must be aborted before attaining escape velocity, the propellant for the payload would be ejected into the stratosphere or the ionosphere (which includes the mesosphere and the thermosphere). The payload propellants may contain up to 2722 kg (6,000 lb) of F_2 or up to 3402 kg (7,500 lb) of N_2O_4. The present report is an evaluation of the effects of these injections on the atmosphere.

The addition of NO and NO_2 to the stratosphere has previously been extensively investigated in the course of evaluating the effects of SST exhaust on the atmosphere. In particular, there is concern about stratospheric ozone levels and the associated shielding of harmful UV-B radiation. Assuming a linear relationship between the stratospheric loading of NO_x and the magnitude of the ozone perturbation, we have calculated the change in ozone expected to result from the space shuttle ejection of N_2O_4, based on the ozone change that is predicted for the (much greater) NO_x input that would accompany large-scale operations of SST's. These calculations show that the effect on ozone is negligibly small.

The N_2O_4 may also be released in the ionosphere. The resulting effects on ion density and composition are discussed. Because of the localized and transient nature of the effects, it is concluded that this will result in no adverse environmental impacts.

Although no previous extensive efforts have been made to evaluate fluorine additions to the atmosphere, other halogens have been considered. In particular, large-scale efforts have gone into the question of chlorine-catalyzed reductions in stratospheric ozone. We have critically reviewed possible stratospheric fluorine reactions to evaluate the magnitude of fluorine-induced ozone destruction relative to the reduction that would be caused by addition of an equal amount of chlorine. Thus, using the magnitude of ozone decrease predicted for chlorine, the decrease in ozone that would result from the fluorine addition has been calculated. Because of the chemical properties of fluorine, and the low concentrations involved, the predicted effect on stratospheric ozone is vanishingly small.

A similar evaluation was made for an ionosphere injection. No adverse environmental impacts are predicted.

References

1. *Chlorofluorocarbons and their Effect on Stratospheric Ozone*, Pollution, Paper No. 5, U.K. Department of the Environment, Central Unit on Environmental Pollution, London, 1976.

2. *Proceedings of the Fourth Conference on the Climatic Impact Assessment Program*, February 4-7, 1975, DOT-TSC-OST-75-38, Department of Transportation, Washington, D.C., 1976.

3. *Environmental Impact of Stratospheric Flight*, National Academy of Sciences, Climatic Impact Committee, Washington, D.C., 1975.

4. *Selected Environmental Impact Studies*, Draft Report, Environmental Research and Technology, Inc., ERT Doc. No. P-3139, Concord, Mass., 1977.

5. *Estimates of Nitric Oxide Production for Lifting Spacecraft Reentry*, Ames Research Center, NASA TM X-62, 052, Moffatt Field, Calif., 1971.

6. *Proceedings of the Space Shuttle Environmental Assessment Workshop on Stratospheric Effects*, March 24-25, 1976, NASA TM X-58198, Houston, Texas, 1977.

7. *Study of High-Altitude Aircraft Wake Dynamics, Task VII*, Rocket Plume Studies, DOT-TST-75-58, Lockheed Palo Alto Research Laboratory, Palo Alto, California, 1974.

8. *Rocket Exhaust Effluent Modeling for Tropospheric Air Quality and Environmental Assessments*, NASA TR-R-473, Marshal Space Flight Center, Huntsville, Ala., 1977.

9. Heicklen, J., *Atmospheric Chemistry*, Academic Press, New York, 1976.

10. *Preliminary Space Shuttle Abort Plan for OFT #1*, Operations Planning Review, Engineering Analysis Division, Johnson Space Center, Houston, Texas, August 22, 1975.

11. Louis, J. F., *Two-Dimensional Transport Model of the Atmosphere*, Thesis, University of Colorado, Boulder, Colorado, 1974.

12. Ratcliffe, J. A., *Physics of the Upper Atmosphere*, Academic Press, New York, 1960.

13. Reiter, E. R., Belmont, A. D., Barrett, E. W., Bauer, E., Gille, J., Lovill, J. E., and Quiroz, R. S., "Stratospheric Climate and its Natural Variability," in *CIAP Monograph 1, The Natural Stratosphere of 1974*, DOT-TST-75-51, Department of Transportation, Washington, D.C., 1951.

14. Yung, Y., personal communication, California Institute of Technology, Pasadena, California, 1977.

15. *U.S. Standard Atmosphere, 1976* NOAA-S/T 76-1562 National Oceanographic and Atmospheric Administration, Washington, D.C., 1976.

16. Jost, W., *Diffusion*, rev. ed., Academic Press, New York, 1960.

17. Bauer, E., "Introduction and Overview: The Stratosphere in its Application to CIAP," in *CIAP Monograph 1, The National Stratosphere of 1974*, DOT-TST-75-51, Department of Transportation, Washington, D.C., 1975.

18. Crutzen, P. J., *Description of a Two-Dimensional Photochemical Model of the Atmosphere Between 980 and 0.415 mb*, submitted for publication (August, 1977). NCAR, Boulder, Colorado.

19. Broderick, A., *Stratospheric Effects from Aviation*, presented at the AIAA/SAE 13th Propulsion Conference, Orlando, Florida, July 11-13, 1977.

20. Rowland, F. S., and Molina, M. J., *Chlorofluoromethanes in the Environment*, Atomic Energy Commission Report No. 1974-1, Washington, D.C., 1974.

21. *Chlorofluoromethanes and the Stratosphere*, NASA Reference Publication 1010, National Aeronautics and Space Administration, Washington, D.C., August 1977.

22. Johnston, H. S., "Photochemistry in the Stratosphere," presented at the Tuneable Laser Conference, Nordfjord, Norway, June 7-11, 1976. Department of Chemistry, University of California, Berkeley.

23. Chang, *Halocarbons*, "Effects on Stratospheric Ozone," National Academy of Sciences, Panel on Atmospheric Chemistry, Washington, D.C., 1976.

24. Bates, D. R., and Hayes, P. B., *Planet. Space Sc.*, Vol. 15, p. 189, 1967.

25. Johnston, H. S., and Selwyn, G. S., *Geophys. Res. Lett.*, Vol. 2, p. 549, 1975.

26. Hampson, R. F., and Garvin, D. ed. *Chemical Kinetic and Photochemical Data for Modelling Atmospheric Chemistry*, NBS Tech. Note 866, 1975.

27. Streit, G. R., Howard, C. J., Schmellekopf, A. L., Davidson, J. A., and Schiff, H. I., J. *Chem. Phys.*, Vol. 65, p. 4761, 1976.

28. Tsang, W., *Int. J. Chem. Kinetics*, Vol. 5, p. 947, 1973.

29. Anastasi, C., and Smith, I. W. M., *J. Chem. Soc. Far. Trans. II*, Vol. 72, p. 1459, 1976.

30. Howard, C. J., and Evenson, K. M., *Geophys. Res. Lett.*, Vol. 4, p. 437, 1977.

31. Broderick, A., "Stratospheric Effects from Aviation," presented at the AIAA/SAE 13th Propulsion Conference, Orlando, Florida, July 11-13, 1977, Paper No. 77-799.

32. Stolarski, R. S., Butler, D. M., and Rundel, R. D., "Uncertainty in Stratospheric Ozone Perturbation Predictions Due to Uncertainties in Reaction Rates," presented at the International Conference on Problems Related to the Stratosphere, Logan, Utah, September 15-17, 1976, in JPL Publication 77-12, Jet Propulsion Laboratory, Pasadena, California, May 15, 1977.

33. Luther, F. M., *Lawrence Livermore Laboratory First Annual Report to the High Altitude Pollution Program*, FAA-EQ-77-6, Department of Transportation, Washington, D.C., 1976.

34. Johnston, H. S., "Analysis of the Independent Variables in the Perturbation of Stratospheric Ozone by Nitrogen Fertilizers," *J. Geophys. Res.*, Vol. 82, p. 1767, 1977.

35. Heicklen, J., *Atmospheric Chemistry*, Academic Press, New York, 1976.

36. Nicolet, N., "The Origin of Nitric Oxide in the Terrestrial Atmosphere, 1970," *Aeron. Aeta*, No. 71.

37. *Chlorofluorocarbons and their Effect on Stratospheric Ozone*, Pollution Paper No. 5, U.K. Department of the Environment, Central Unit on Environmental Pollution, 1976.

38. Rowland, F. S., and Molina, M. J., *Chlorofluoromethanes in the Environment*, Atomic Energy Commission Report No. 1974-1, 1974.

39. Stolarski, R. S., and Rundel, R. D., *Geophys. Res. Lett.*, Vol. 2, p. 443, 1975.

40. Zander R., Poland, G., and Delbonille, L., *Geophys. Res. Lett.* Vol. 4, p. 117, 1977.

41. Morz, E. J., Lazrus, A. L., and Bonelli, J. F., *Geophys. Res. Lett.*, Vol. 4, p. 149, 1977.

42. Farmer, C. B., and Raper, O. F., *The HF/HCl Ratio in the 14-38 km Region of the Stratosphere*, in press (1977).

43. Raper, O.F., personnal communication, 1977.

44. Albright, R. C., Dodonov, A. F., Lavrovskaya, G. K., Morozov, I. I., and Tal'roze, V. L., *J. Chem Phys.*, Vol. 50, p. 3632, 1969.

45. Rabidean, S. W., Hecht, H. G., and Lewis, W. B., *J. Magn. Reson.*, Vol. 6, p. 384, 1972.

46. Rapp, D., and Johnson, H., *J. Chem. Phys.*, Vol. 33, p. 695, 1960.

47. Kim, P., Macdean, D. I., and Valance, W. G., NTIS. AD. 751456. *Abstracts of the 164th ACS National Meeting*, 1972.

48. Gg Wagner, H., Zetzsch, C., and Warnatz, J., *Ber. Bunsenges. Phys. Chem.*, Vol. 76, p. 526, 1972.

49. C., Zetzsch, *European Symposium of the Combustion Institute.* Edited by F. S. Weinberg. Academic Press, London, Vol. 35, 1973.

50. Arutyunov, V. S., Popov, L. S., and Chaikin, A. M., *Kinet. Katal.*, Vol. 17, p. 286, 1976.

51. Chen, H. L., Trainor, D. W., Center, R. E., and Fyfe, W. I., *J. Chem. Phys.*, Vol. 12, p. 5513, 1977.

52. Clyne, M. A. A., and Watson, R. T., *J. Chem. Soc., Faraday Trans. I*, Vol. 70, p. 1109, 1974.

53. Homann, K. H., Solomon, W. C., Warnatz, J., Gg Wagner, H., and Zetzsch, C., *Ber Bunsenges. Phys. Chem.*, Vol. 74, p. 585, 1970.

54. Dodonov, A. F., Lavrovskaya, G. K., Morozov, I. I., Tal'roze, V. L., *Doki., Akod. Nauk USSR*, Vol. 198, p. 622, 1971; *Doki Phys., Chem.* (English Trans.), Vol. 198, p. 440, 1971.

55. Foon, R., and Reid, G. P., *Trans. Faraday Soc.*, Vol. 67, p. 3513, 1971.

56. Bozzelli, J., Thesis, Dept. of Chemistry, Princeton University, 1972.

57. Kompa, K. L., Wanner, J., *Chem. Phys. Lett.*, Vol. 12, p. 560, 1972.

58. Rabideau, S. W., Hecht, H. G., and Lewis, W. B., *J. Magn. Reson.*, Vol. 6, p. 384, 1972.

59. Clyne, M. A. A., McKenney, D. J., and Walker, R. F., *Can. J. Chem.*, Vol. 51, p. 3596, 1973.

60. Igoshin, V. I., Kulakov, L. V., and Nikitin, A. I., *Sov. J. Quant. Electron.*, Vol. 3, p. 306, 1974.

61. My, Lam Thank., Peyron, M., and Puget, P., J. Chem. Phys., Vol. 71, p. 377, 1974.

62. Zetzsch, C., Ph.D. Dissertation, Georg-August University, Gottinger, 1971.

63. Fettis, G. C., and Knox, J. H., *Progress in Reaction Kinetics*, Vol. 2, p. . 1964.

64. Gg Wagner, H., Warnatz, J., and Zetzsch, C., *An. Assoc. Quin. Argent.*, Vol. 59, p. 169, 1971.

65. Pollock, T. L., and Jones, W. E., Can. J. Chem., Vol. 51, p. 2041, 1973.

66. Staricco, E. H., Sicre, S. E., and Schumacher, H. J., *Z. Physik. Chem. N. F.*, Vol. 31, p. 385, 1962.

67. Steunenberg, R. K., and Vogel, R. C., *J. Am. Chem. Soc.* Vol. 78, p. 901, 1956.

68. Nagy, A. F., Liu, S. C., and Baker, D. J., *Geophys. Res. Lett.*, Vol. 3, p. 731, 1976.

69. Heicklen, J., *Atmospheric Chemistry*, Academic Press, New York, 1976.